



**HAL**  
open science

# Advanced kriging-based surrogate modelling and sensitivity analysis for rotordynamics with uncertainties

Enora Denimal, Jean-Jacques Sinou

## ► To cite this version:

Enora Denimal, Jean-Jacques Sinou. Advanced kriging-based surrogate modelling and sensitivity analysis for rotordynamics with uncertainties. *European Journal of Mechanics - A/Solids*, 2021, 90, pp.1-20. 10.1016/j.euromechsol.2021.104331 . hal-03246852

**HAL Id: hal-03246852**

**<https://inria.hal.science/hal-03246852>**

Submitted on 7 Jun 2021

**HAL** is a multi-disciplinary open access archive for the deposit and dissemination of scientific research documents, whether they are published or not. The documents may come from teaching and research institutions in France or abroad, or from public or private research centers.

L'archive ouverte pluridisciplinaire **HAL**, est destinée au dépôt et à la diffusion de documents scientifiques de niveau recherche, publiés ou non, émanant des établissements d'enseignement et de recherche français ou étrangers, des laboratoires publics ou privés.



## Advanced kriging-based surrogate modelling and sensitivity analysis for rotordynamics with uncertainties

E. Denimal<sup>a,\*</sup>, J.-J. Sinou<sup>b,c</sup>

<sup>a</sup> Univ. Gustave Eiffel, Inria, COSYS/SII, I4S, Campus de Beaulieu, 35042 Rennes, France

<sup>b</sup> Laboratoire de Tribologie et Dynamique des Systèmes, UMR CNRS 5513, École Centrale de Lyon, 36 avenue Guy de Collongue 69134 Écully Cedex, France

<sup>c</sup> Institut Universitaire de France, 75005 Paris, France

### ARTICLE INFO

#### Keywords:

Rotordynamics  
Hybrid uncertainties  
Polynomial chaos expansion  
Kriging meta-modelling

### ABSTRACT

Rotating machinery are present in many engineering applications. Such rotor systems often subjected to high vibration loads that can be at the origin of noise or failure. For these reasons, it is of main importance to predict with accuracy the critical speeds and the dynamic response amplitude of such structures. However, they are often subjected to many potential uncertainties that may rise from environmental variations or manufacturing tolerances. These uncertain parameters, often described as random, are often numerous and must be taken into consideration during the design stage. For this, some design parameters are usually adjusted to propose a robust design of the rotor, considering the possible variation of the random parameters. Performing such studies require to be able to deal with a high number of uncertain parameters and with parameters of different nature, namely parametric and random.

This work proposes to illustrate the efficiency of advanced kriging-based surrogate modelling in order to achieve such a goal. The proposed hybrid surrogate-model combines polynomial chaos expansion and kriging to deal with both parameter natures, to consider nine varying parameters of a full finite element model of the rotating system under study. For the first time, this hybrid surrogate model is applied to perform rotordynamics analysis and more specifically the prediction of critical speeds and the associated unbalance responses for a complex rotor system with uncertainties. Compared to previous works, the kriging performances are significantly increased by integrating some physical properties of the rotor directly in its construction. Finally, the hybrid surrogate model gives a direct access to the Sobol indices which makes it possible to carry out without additional computation costs an extensive sensitivity analysis.

### 1. Introduction

Rotating machinery is a major component in many structures in the field of aeronautics or energy. The analysis of such component is essential to reduce noise and vibration and requests the use of specific tools. Even if many faults can lead to increase the vibration signatures of a rotor system, one of the chief concern of engineers who design large rotors is to be able to predict the critical speeds that correspond to the speeds of rotation (or frequencies) for which the amplitude of vibration often passes through a maximum. The capability of estimating these vibration amplitudes that are commonly excited by unbalance of the rotating structure is also a crucial point for a robust design of rotating machinery. Indeed, if the amplitude of vibration at one or more critical speeds is excessive, then catastrophic dysfunctions or failures may occur. The key point for engineers is to detect these potential problems highlighted and find ways to prevent them if possible.

However, this is not necessarily easy because the vibratory behaviour of the rotating machinery is dependent on many geometrical parameters and materials of the different elements of a rotor system, such as the rotor shaft, discs and flexible bearing supports for example. Being able to have a global vision of the impact of each part of a rotating system and to prejudge the effect of the variability of certain parameters must be studied in detail and considered while designing. As a result, one of the most interesting but also difficult challenges is to improve the understanding of the dynamic behaviour of rotating structures by integrating the uncertainties present in the models. One of the most important tasks is to be able to develop methods that guarantee the numerical feasibility for mechanical systems with many degrees of freedom and subject to various uncertainties of potentially different types.

There are many software packages that are capable of solving the rotor dynamic system for design purposes. Such codes can be easily

\* Corresponding author.

E-mail addresses: [enora.denimal@inria.fr](mailto:enora.denimal@inria.fr) (E. Denimal), [jean-jacques.sinou@ec-lyon.fr](mailto:jean-jacques.sinou@ec-lyon.fr) (J.-J. Sinou).

used by engineers and make it possible to test various designs by adding or modifying some parts of the mechanical assembly such as the supporting structure (i.e. stator parts) and one or more rotating structures (i.e. rotor parts). One of the current major limitations of commercial software developed for design and analysis of rotor dynamics is the ability to quickly conduct numerous studies in a short time in order to define the most efficient and reliable rotor system according to a set of specifications. In recent years, advanced numerical methods have been developed to approximate the vibration behaviour of such systems for a predefined design space while drastically reducing calculation times. Generally the main motivation is to significantly reduce computation effort when evaluating the design space of interest.

When designing a system, engineers face numerous uncertain parameters of different natures. Indeed, geometrical or material properties of a rotor vary due to manufacturing tolerances or due to environmental variations. These parameters are usually described by a random law and must be taken into consideration during the design process as the rotor must be robust to these possible variations. A few key design parameters are usually identified and adjusted to meet the conception requirements. They can take value in a predefined interval and engineers tune these values based on user-knowledge or using large parametric studies. Due to a limited amount of numerical resources, only a few simulations of the rotor dynamic for these parameters are conducted and the behaviour on the total design space is deduced from these few evaluations. It creates an uncertainty, called *epistemic*, as it could be reduced by increasing the number of simulations. When dealing with realistic models, the number of uncertain parameters (random and parametric) quickly increases and specific advanced numerical methods must be considered to take them into account simultaneously with an affordable computational time.

Traditional methods for uncertainty propagation are based on a unique description of the uncertainty (random, parametric, interval, fuzzy etc.), and depending on this description, different types of approaches are preferably employed to propagate it. For example, perturbation methods or Polynomial Chaos Expansion (PCE) are well adapted for random uncertainties. Hence, PCE has largely been used to predict the critical speeds and mode shapes of rotor systems (Sarrouy et al., 2012) or the vibration amplitudes of linear or nonlinear rotor systems (Didier et al., 2012a,b; Sinou et al., 2015; Sinou and Jacquelin, 2015; Jacquelin et al., 2016; Yongfeng et al., 2019; Garoli and de Castro, 2020; Zhang et al., 2020; Fu et al., 2020). Recently, kriging models have drawn much attention in the field of rotordynamics and have been sometimes used for rotating machinery diagnoses (Wang et al., 2018a; Lu et al., 2019), parameter identification of rotor-bearing systems (Han et al., 2013, 2017), vibration analysis of bearings or rotating machinery (Sinou et al., 2018; Barbosa and Alves, 2019; Barbosa et al., 2020) or design optimization of an aero-engine turbine disc (Huang et al., 2011). However, as raised previously, random and parametric uncertainties are usually present simultaneously and adopting a unique modelling might not be the best numerical strategy. Recent works have proposed hybrid methods associating different methods to achieve a better modelling of the uncertainties (Lü and Yu, 2016; Wu et al., 2017; Wang et al., 2018b; Denimal et al., 2018; Zheng et al., 2019). More specifically, in Denimal et al. (2018), the authors proposed an approach that associate kriging and PCE to model random and parametric uncertainties simultaneously. This method was introduced and validated on a phenomenological model of friction induced vibrations to predict its stability. If this approach worked well on a model with a low number of degrees of freedom and a small number of uncertain parameters, its extension to large and realistic finite element models with a higher number of uncertain parameters has to be proven as it implies a higher numerical cost.

This paper proposes to continue the initial previous work of Sinou et al. (2018) that focused on an illustration of the classical use of kriging meta-modelling in the field of rotordynamics. In this previous work, Monte Carlo Simulations (MCS) were performed to estimate the average

and the variance of the critical speeds and of the associated vibration amplitudes. Classic kriging was then used to predict their evolution considering some varying parameters. One of the major advances and contributions of the proposed study is to extend kriging models by combining kriging with a strategy of propagating uncertainties through PCE to avoid MCS simulation and thus reduce the computational cost. In addition, the study highlights the potential of the approach and strategy developed by illustrating the ability to conduct sensitivity studies without additional numerical calculation costs. Finally, an improvement of the kriging meta-modelling is proposed by introducing the symmetrical properties of the rotor directly in the meta-model.

The paper is organized as follows. First, a brief description of the rotor system under study and the chosen uncertain parameters are presented. Then, the proposed methodology based on the effective use of hybrid meta-modelling by associating the PCE and the kriging formalisms are discussed. One specific attention will be paid to promote the use of specific kriging constructions to reduce the number of samples required and consequently the computational times. Finally, efficiency and accuracy of the hybrid uncertainty propagation and quantification on the prediction of the critical speeds and the associated amplitudes is evaluated and commented. Additionally, efficiency of the proposed approach to accuracy conduct a sensitivity analysis without significant additional calculations is illustrated.

## 2. Description of the rotor system

This section briefly presents the modelling of the rotor system used in the subsequent analysis. The model under study is composed of a shaft and four discs, represented in Fig. 1(a). It is supported by two flexible supports, one on each extremity. An unbalanced mass is located on the first disc. The modelling of each part is briefly presented in the following sections (Friswell et al., 2010).

### 2.1. Shaft modelling

The shaft is modelled with a Finite Element Model (FEM) composed of ten Euler beam elements. The elementary element is displayed in Fig. 1(b) where each node has four degrees of freedom, namely two lateral displacements  $v$  and  $w$  and two rotations  $\theta$  and  $\psi$ . The nodal displacement vector in the fixed frame of the element  $i$  is  $\delta^{(s,i)} = [v_1 \ w_1 \ \theta_1 \ \psi_1 \ v_2 \ w_2 \ \theta_2 \ \psi_2]^T$ . The equation of motion of the  $i$ th element writes:

$$\left( \mathbf{M}_R^{(s,i)} + \mathbf{M}_T^{(s,i)} \right) \ddot{\delta}^{(s,i)} + \left( \mathbf{C}^{(s,i)} + \omega \mathbf{G}^{(s,i)} \right) \dot{\delta}^{(s,i)} + \mathbf{K}^{(s,i)} \delta^{(s,i)} = \mathbf{0} \quad (1)$$

where  $\mathbf{M}_R^{(s,i)}$  and  $\mathbf{M}_T^{(s,i)}$  are the rotational and translational mass matrices of the element  $i$ ,  $\mathbf{C}^{(s,i)}$  is the damping matrix of the element  $i$ ,  $\mathbf{G}^{(s,i)}$  is the gyroscopic matrix of the element  $i$  and  $\mathbf{K}^{(s,i)}$  is the stiffness matrix of the element  $i$ . The dot denotes the derivative with regard to time.

The geometrical and material properties of the shaft are given in Table 1.

**Table 1**  
Geometrical and material properties of the shaft.

Notation	Parameter name	Value
$R^s$	Rotor shaft radius	0.02 m
$L^s$	Rotor shaft length	1 m
$E^s$	Young's modulus of shaft material	$2.1 \cdot 10^{11}$ N/m <sup>2</sup>
$G^s$	Shear modulus of shaft material	$7.7 \cdot 10^{10}$ N/m <sup>2</sup>
$\rho^s$	Density of shaft material	7800 kg/m <sup>3</sup>
$\nu^s$	Poisson ratio of shaft material	0.3

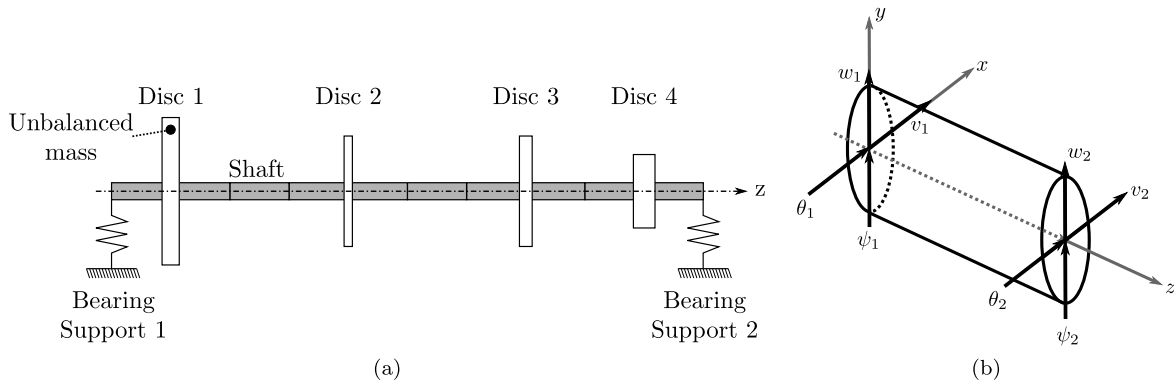


Fig. 1. Model under study (a) and variables for shaft elementary elements (b).

### 2.2. Discs modelling and unbalance forces

The four discs are modelled as rigid discs. The nodal displacements of the disc  $j$  in the fixed frame are denoted  $\delta^{(d,j)} = [u \ v \ \theta \ \psi]^T$ . The corresponding equation of motion writes:

$$\left( \mathbf{M}_R^{(d,j)} + \mathbf{M}_T^{(d,j)} \right) \ddot{\delta}^{(d,j)} + \omega \mathbf{G}^{(d,j)} \dot{\delta}^{(d,j)} = \mathbf{F}^{(d,j)} \quad (2)$$

where  $\mathbf{M}_R^{(d,j)}$  and  $\mathbf{M}_T^{(d,j)}$  are the rotational and translational mass matrices of the disc  $j$  respectively, and  $\mathbf{G}^{(d,j)}$  is the gyroscopic matrix of the disc  $j$ . The discs geometrical properties are given in Table 2.  $\mathbf{F}^{(d,j)}$  defines the unbalance of the disc  $j$ . For the proposed study, only a residual unbalanced mass located on the disc 1 is assumed. The former is modelled as a periodic load of the form:

$$\mathbf{F}^{(d,1)}(t) = [m_u d_u \omega^2 \cos(\omega t + \phi) \quad m_u d_u \omega^2 \sin(\omega t + \phi) \quad 0 \quad 0]^T \quad (3)$$

where  $m_u$  and  $d_u$  are the mass unbalance and eccentricity, respectively.  $\phi$  is the initial angular position of the mass with respect to the  $z$ -axis.  $\omega$  defines the rotational speed of the rotor. The discs geometrical properties and the characteristics of the unbalance force are given in Table 2.

### 2.3. Flexible supports

The flexible bearing supports are modelled as two linear springs, one in each direction of the fixed frame. The vertical and horizontal stiffness of the first bearing support (the second bearing support, respectively) are denoted  $k_v^{(b,1)}$  and  $k_h^{(b,1)}$  ( $k_v^{(b,2)}$  and  $k_h^{(b,2)}$ , respectively) respectively. The corresponding global matrices are denoted  $\mathbf{K}^{(b,1)}$  and  $\mathbf{K}^{(b,2)}$ . For the sake of simplicity, damping and rotational contributions are neglected (see Table 3).

Table 2  
Geometrical and material properties of the discs.

Notation	Parameter name	Value
$R^1$	Outer radius — Disc 1	0.25 m
$e^1$	Thickness — Disc 1	0.03 m
$R^2$	Outer radius — Disc 2	0.1875 m
$e^2$	Thickness — Disc 2	0.015 m
$R^3$	Outer radius — Disc 3	0.1875 m
$e^3$	Thickness — Disc 3	0.0225 m
$R^4$	Outer radius — Disc 4	0.125 m
$e^4$	Thickness — Disc 4	0.0375 m
$E^S$	Young's modulus of discs material	$2.1 \cdot 10^{11}$ N/m <sup>2</sup>
$\rho^S$	Density of discs material	7800 kg/m <sup>3</sup>
$m_u$	Mass unbalance — Disc 1	0.01 kg
$d_u$	Eccentricity of the unbalanced mass — Disc 1	0.01 m

### 2.3.1. General equation of the rotor system

The general global matrices are assembled by summing the contributions of the different components (i.e. the rotor shaft, the four discs, the two flexible bearing supports and the unbalance force). The global equation of motion of the FEM of the rotor system is then given by:

$$\mathbf{M}\ddot{\mathbf{x}} + (\mathbf{C} + \omega \mathbf{G})\dot{\mathbf{x}} + \mathbf{K}\mathbf{x} = \mathbf{F} \quad (4)$$

where  $\mathbf{x}$  is the displacement vector of the rotor system. The matrix  $\mathbf{M}$  includes mass matrices of each shaft element  $\mathbf{M}_R^{(s)}$  and  $\mathbf{M}_T^{(s)}$  and the four rigid discs  $\mathbf{M}_R^{(d,j)}$  and  $\mathbf{M}_T^{(d,j)}$  (for  $j = 1, \dots, 4$ ). The matrix  $\mathbf{G}$  includes gyroscopic matrices of each shaft element  $\mathbf{G}^{(s)}$  and the four rigid discs  $\mathbf{G}^{(d,j)}$  (for  $j = 1, \dots, 4$ ).

The matrix  $\mathbf{K}$  includes the stiffness matrices of each shaft element  $\mathbf{K}^{(s)}$  and supports  $\mathbf{K}^{(b,1)}$  and  $\mathbf{K}^{(b,2)}$ . The matrix  $\mathbf{C}$  considers the shaft internal damping of each element  $\mathbf{C}^{(s)}$  and  $\mathbf{F}$  is the vector of unbalance force including the contribution  $\mathbf{F}^{(d,1)}(t)$ .

For the reader more specifically specialized in rotor dynamics, it is worth noting that the model proposed in this study may appear simple on some aspects (geometry of the complete rotor, Euler beams formulation instead of Timoshenko, no damping coefficients or cross coupling coefficients for the bearing supports, ...). Therefore many effects of the rotor-bearing system are not considered due to the model adopted and out of the scope of the proposed study. Indeed, the main objective of this study is to illustrate the potential of an efficient hybrid meta-modelling and methodology for uncertainty propagation in the field of rotordynamics.

## 3. Efficient hybrid meta-modelling and methodology for uncertainty propagation

The main objective of this section is to describe the proposed methodology to promote the effective use of hybrid meta-modelling for predicting the vibrational behaviour of rotating systems (i.e. the critical speeds and the associated vibration amplitudes) in the presence of uncertainties. One of the major contributions of this section is to highlight how it is possible to improve kriging predictions and performances by modifying the regression or the construction strategy to take into account the physical properties of the problem under study.

Table 3  
Properties of the flexible bearing supports.

Notation	Parameter name	Value
$k_v^{(b,1)}$	Vertical stiffness — Bearing 1	$3 \cdot 10^6$ N/m
$k_h^{(b,1)}$	Horizontal stiffness — Bearing 1	$3 \cdot 10^6$ N/m
$k_v^{(b,2)}$	Vertical stiffness — Bearing 2	$[0.1; 2] \cdot 10^6$ N/m
$k_h^{(b,2)}$	Horizontal stiffness — Bearing 2	$[0.1; 2] \cdot 10^6$ N/m

In order to achieve such an objective, the uncertain parameters chosen for the rotor system under study and the definition of the physical quantities to be predicted are firstly described. In a second time, the mathematical formulation of the proposed hybrid meta-model based on the combination of the PCE and the kriging meta-modelling is discussed: the use of the PCE (for uncertainty related to the random parameters) and the kriging meta-modelling (for uncertainty related to the parametric parameters) is described. In addition, the possibility of optimizing the kriging construction for a symmetrical problem is discussed. The last part of this section is devoted to the exploitation of the PCE in order to obtain the statistical moments of the outputs (i.e. mean and variance), as well as the Sobol indices.

### 3.1. Uncertain parameters

Two types of uncertain parameters are considered in the present study. The first type corresponds to random parameters described by a Probability Density Function (PDF). These uncertainties might come from manufacturing tolerances but also from modifications due to environmental considerations or from a potential lack of precise knowledge for specific physical parameters.

Seven parameters describing the rotor system are random. They are summarized in Table 4 where the % of variation around their mean value is also given. It can be noted that the values chosen for variation of geometric amount is higher than classical tolerances adopted in manufacturing process. The values chosen correspond more to the case of a lack of precise knowledge of the input data and the main objective is to demonstrate the efficiency and robustness of the proposed approach in the presence of uncertainties that have a strong impact on both the critical speeds and unbalance responses of the rotor system. Additionally, the choice of the seven random parameters is made so that they have a different impact on the rotor system. Indeed they provide specific and different modifications on the mass and stiffness contributions, as well as on the gyroscopic effects. Moreover, these seven parameters have spatially different modifications on the rotor. Indeed, the Young modulus of the rotor shaft is a parameter that has an influence on the full model (with a random contribution on all degrees of freedom of the FEM model), whereas the disc thicknesses and the bearing stiffnesses are more localized (with random contributions only located at the specific degrees of freedom of the four discs and the two bearing supports). A uniform distribution is taken here as no information is available for a more precise description. However, the proposed strategy remains valid for other distributions. We recall that the main objective of the proposed study is to illustrate the effectiveness and robustness of the proposed approach in the presence of uncertainties that potentially have a strong impact on the critical speeds and unbalance responses of the rotor system.

The second type of uncertain parameters are considered as deterministic and corresponds to the stiffnesses of the second bearing support (i.e.  $k_v^{b,2}$  and  $k_h^{b,2}$ ) and can take value in  $[0.1, 2] \times 10^6$  N/m. This choice is guided by the fact that we intend to demonstrate the interest and feasibility of proposing optimized kriging strategies that use symmetry properties on the output results obtained with respect to the parametric input parameters (i.e.  $k_h^{b,2}$  and  $k_v^{b,2}$  in the present case). The final objective is to assess the rotor forward and backward critical speeds and the associated vibration amplitudes when these two bearing stiffnesses are varying independently and while considering the uncertainty of the seven random parameters.

### 3.2. Physical parameters to predict

As previously stated, the objective of the present study is to develop efficient kriging meta-modellings for estimating the critical speeds and the associated vibration amplitudes with uncertainties. Due to the fact that the critical speeds of a rotating machine occur when the rotational

**Table 4**  
Random parameters description.

Parameter name	Notation	% variation	Law
Young modulus shaft	$E$	$\pm 5\%$	Uniform
Thickness — Disc 1	$e_1$	$\pm 10\%$	Uniform
Thickness — Disc 2	$e_2$	$\pm 10\%$	Uniform
Thickness — Disc 3	$e_3$	$\pm 10\%$	Uniform
Thickness — Disc 4	$e_4$	$\pm 10\%$	Uniform
Horizontal stiffness — Bearing 1	$k_h^{b,1}$	$\pm 5\%$	Uniform
Vertical stiffness — Bearing 1	$k_v^{b,1}$	$\pm 5\%$	Uniform

speed matches its natural frequencies, the Campbell diagram that represents the frequency versus the rotation speed of the rotor system is used to evaluate these critical speeds. Additionally, the vibration amplitudes are estimated by performing a classical unbalance response of the rotor system, as defined in Eq. (4). More specifically, the studies conducted will focus on the eight critical speeds  $(f^i)_{i \in [1,8]}$  as well as the associated vibration amplitudes  $(a^i)_{i \in [1,8]}$  for all the stiffness values of the second bearing support and considering the seven random parameters. For the sake of clarity and readability, the eight critical speeds are numbered from 1 to 8 by ascending values and no distinction will be made in the notations for the backward and forward modes.

These critical speeds  $(f^i)_{i \in [1,8]}$  as well as the associated vibration amplitudes  $(a^i)_{i \in [1,8]}$  depend on the nine varying parameters, i.e. the seven random parameters  $(E, e_1, e_2, e_3, e_4, k_v^{b,1}, k_h^{b,1})$  plus the two deterministic varying parameters  $(k_v^{b,2}, k_h^{b,2})$ . So the explicit functions write:

$$f^i(\mathbf{x}, \xi) \quad \text{and} \quad a^i(\mathbf{x}, \xi) \quad (5)$$

where  $\mathbf{x} = [k_h^{b,2}, k_v^{b,2}]$  is the vector of the parametric parameters, and  $\xi = [\xi_E, \xi_{e_1}, \xi_{e_2}, \xi_{e_3}, \xi_{e_4}, \xi_{k_h^{b,1}}, \xi_{k_v^{b,1}}]$  is the vector of the random parameters.

As the parameters are of different natures, different meta-modelling approaches will be employed: PCE for the random parameters and kriging for the parametric parameters. Both methods are explained in the following as well as the mathematical formulation of the final hybrid meta-model.

### 3.3. Polynomial chaos expansion

The uncertainty related to the random parameters  $\xi = [\xi_E, \xi_{e_1}, \xi_{e_2}, \xi_{e_3}, \xi_{e_4}, \xi_{k_h^{b,1}}, \xi_{k_v^{b,1}}]$  is modelled and propagated with a PCE as it gives a stochastic description of the uncertainty. All parameters follow the same distribution, namely the uniform distribution. According to the PCE theory, a random parameter  $\Gamma$  can be approximated by a convergent, in the  $\mathcal{L}^2$  sense, expansion (Wiener, 1938; Sudret, 2008; Xiu and Karniadakis, 2002):

$$\Gamma(\xi) = \sum_{k=0}^{P-1} \gamma_k \Phi_{\alpha_k}(\xi) \quad (6)$$

where the  $\Phi_{\alpha_k}(\xi)$  are the multivariate orthogonal polynomials and  $(\gamma_k)$  the weighting coefficients. For practical reasons, the expansion is truncated and  $P$  terms are kept. Only polynomials of order inferior to the chaos order  $m$  are kept, and without a selection scheme the number of terms is  $P = \binom{m+r}{m}$  with  $r$  the number of random parameters (here  $r = 7$ ). One can clearly see here that with such a high number of random parameters, the number of terms in the polynomial basis explodes quickly, which refers to the well known ‘‘computational burden’’ of the PCE.

The multi-variate orthogonal polynomial basis  $(\Phi_{\alpha_k})$  is obtained by tensorisation of mono-variate orthogonal polynomial sets  $(\Psi_{\alpha}^{(i)})$ , where  $\alpha$  is the polynomial order and  $i \in [E, e_1, e_2, e_3, e_4, k_h^{b,1}, k_v^{b,1}]$ . The mono-variate polynomial basis related to the parameter  $i$  is given by the Askey scheme (Xiu and Karniadakis, 2002), which gives the correspondence between the classical distributions and the associated orthogonal

polynomial basis. As only uniform laws are considered here, Legendre polynomials are employed. Hence, if  $\alpha = (\alpha_E, \alpha_{e_1}, \alpha_{e_2}, \alpha_{e_3}, \alpha_{e_4}, \alpha_{k_h^{b,1}}, \alpha_{k_v^{b,1}})$  is the multivariate index of the multi-variate polynomial  $\Phi_\alpha$ , it writes:

$$\Phi_\alpha(\xi) = \Psi_{\alpha_E}^{(E)}(\xi_E) \times \dots \times \Psi_{\alpha_{k_v^{b,1}}}^{(k_v^{b,1})}(\xi_{k_v^{b,1}}) \quad (7)$$

and the order of  $(\Phi_\alpha)$  is equal to  $\sum_i \alpha_i$  with  $i \in [E, e_1, e_2, e_3, e_4, k_h^{b,1}, k_v^{b,1}]$ .

To reduce the number of terms in the PCE and avoid convergence issues, a hyperbolic truncation norm is adopted to select a subset of polynomials with low order interactions (Blatman and Sudret, 2011; Denimal et al., 2018):

$$\|\alpha\| = \left( \sum_{i \in [E, e_1, e_2, e_3, e_4, k_h^{b,1}, k_v^{b,1}]} \alpha_i^q \right)^{1/q} \leq m \quad (8)$$

where  $q \in (0, 1]$  is fixed by the user. The lower it is, the smaller is the PCE basis. Such a norm is based on the idea that the main effects are governed by low order interactions between the different parameters. As an illustration, a two-dimensional case is illustrated in Fig. 2 where the polynomials kept in the expansion are given. A black point of coordinates  $(n, m)$  means that the polynomial of degree  $n$  w.r.t. the variable  $x_1$  and of degree  $m$  w.r.t. the variable  $x_2$  is kept in the expansion. As one can see, when  $q$  increases, less and less terms are kept in the expansion and only terms with low order interactions are kept.

The choice of the chaos order  $m$  and of the hyperbolic norm  $q$  depends on each case. Some automatic error criterion as the Leave-One-Out (LOO) (Blatman and Sudret, 2011; Denimal et al., 2019) might be used to guide the users without any additional computation. However the most reliable criterion remains the comparison with a reference set (when it is possible to compute it).

Intrusive and non-intrusive approaches can be used to compute the coefficients  $(\gamma_k)$  (Blatman and Sudret, 2011; Sudret, 2008). A non-intrusive approach based on the regression is employed here. The coefficients  $(\gamma_k)$  are the solution of a least-square minimization problem between the random function  $\Gamma(\xi)$  and its PCE approximation at  $N$  points. This experimental design is build based on an LHS to generate the input space.

### 3.4. Kriging

#### 3.4.1. General formulation

The uncertainty related to the parametric parameters  $\mathbf{x} = (k_h^{b,2}, k_v^{b,2})$  will be modelled with a kriging meta-model. This uncertainty is epistemic as only a limited amount of data are available due to the numerical cost. Each PCE coefficient can be seen as a function of the parametric parameters. For the sake of readability in the following,  $\gamma$  will denote one PCE coefficient. The process is applied for each coefficient of each created PCE. Each PCE coefficient is then approximated with a kriging approximation (Matheron, 1962; Lophaven et al., 2002):

$$\gamma(\mathbf{x}) = \mathbf{g}(\mathbf{x})^T \boldsymbol{\beta} + Z(\mathbf{x}) \quad (9)$$

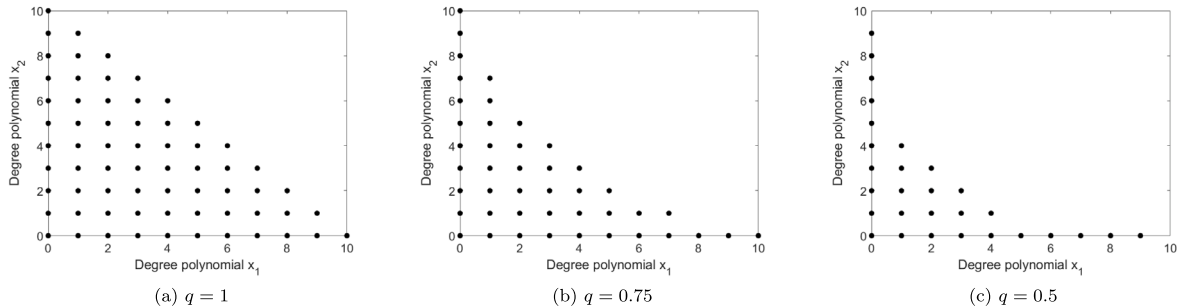


Fig. 2. Illustration of the truncation strategy based on the hyperbolic norm in dimension 2 — (•): polynomials kept in the PCE expansion.

Table 5

Examples of correlation function family in dimension 1.

Kernel	$k(\theta, d)$
Gaussian	$\exp\left(-\frac{d^2}{2\theta^2}\right)$
Exponential	$\exp\left(-\frac{ d }{\theta}\right)$
Matérn 5/2	$\left(1 + \frac{\sqrt{5} d }{\theta} + \frac{5d^2}{3\theta^2}\right) \exp\left(-\frac{\sqrt{5} d }{\theta}\right)$
Matérn 3/2	$\left(1 + \frac{\sqrt{3} d }{\theta}\right) \exp\left(-\frac{\sqrt{3} d }{\theta}\right)$
Linear	$\max(0, 1 - \frac{ d }{\theta})$
Spherical	$1 - 1.5y + 0.5y^3$ , with $y = \min(1, \frac{ d }{\theta})$
Spline	$\begin{cases} 1 - 15\left(\frac{ d }{\theta}\right)^2 + 30\left(\frac{ d }{\theta}\right)^3 & \text{for } 0 \leq \frac{ d }{\theta} \leq 0.2 \\ 1.25\left(1 - \frac{ d }{\theta}\right)^3 & \text{for } 0.2 < \frac{ d }{\theta} < 1 \\ 0 & \text{for } \frac{ d }{\theta} \geq 1 \end{cases}$

where  $\mathbf{g}$  is a set of  $n_r$  regressive functions often chosen as polynomial of low order,  $\boldsymbol{\beta}$  are the weighting coefficients and are solution of a least square problem. The regression part corresponds to the general trend and describe a global evolution.  $Z$  is a zero mean Gaussian process of variance  $\sigma^2$ , it usually corresponds to more local evolution. Its covariance matrix is:

$$\mathbb{E}[Z(\mathbf{x}'), Z(\mathbf{x})] = \sigma^2 \mathcal{R}(\theta, \mathbf{x}', \mathbf{x}) \quad (10)$$

where  $\mathcal{R}$  is the spatial correlation function of scaling parameter  $\theta$ , and  $\mathbf{x}'$  and  $\mathbf{x}$  are two points of the design space. For an anisotropic kriging, the dimension of  $\theta$  is the dimension of the input space (here 2). The use of a spatial correlation function translates the idea that two points that are close in the input space, have similar behaviour in the output space. The multi-variate correlation function  $\mathcal{R}$  is build by taking the product of a mono-variate correlation family (Lophaven et al., 2002; Williams and Rasmussen, 2006). It writes in the case of dimension  $d$ :

$$\mathcal{R}(\theta, \mathbf{x}', \mathbf{x}) = \prod_{j=1}^d \mathcal{R}_j(\theta_j, d_j) \quad (11)$$

where the  $\mathcal{R}_j$  is a 1D-correlation functions taken in Table 5,  $\theta_j$  is the value of  $\theta$  in dimension  $j$  and  $d_j = x'_j - x_j$  is the distance between  $\mathbf{x}$  and  $\mathbf{x}'$  in the  $j$ th dimension.

To build a kriging meta-model,  $Q$  evaluations of the expensive function are required. It defines a set of  $Q$  inputs  $(\mathbf{x}^{(i)})_{i \in [1, Q]}$  and their evaluation  $(\gamma^{(i)} = \gamma(\mathbf{x}^{(i)}))_{i \in [1, Q]}$ . This set is called experimental design. From this set, the regression matrix  $\mathbf{G}$  of coefficients  $G_{i,j} = g_j(\mathbf{x}^{(i)})$  and the correlation matrix  $\mathbf{R}$  of coefficients  $R_{i,j} = \mathcal{R}(\theta, \mathbf{x}^{(i)}, \mathbf{x}^{(j)})$  can be determined. Finally,  $\boldsymbol{\beta}$  is calculated by solving a likelihood optimization problem, from which  $\boldsymbol{\beta}$  and  $\sigma^2$  are deduced. The interested reader can refer to Lophaven et al. (2002) for a detailed description of all the mathematical developments and the numerical implementation.

The quality of a kriging meta-model relies on the choice of the correlation function, the choice of the regression part and the quality of the learning set. In the current study, the experimental design is based on an LHS for which a maximin criterion has been optimized to ensure an homogeneous distribution of the points in the input space (Dupuy et al., 2015; Forrester et al., 2008). The kriging construction is based on the DACE toolbox (Lophaven et al., 2002).

### 3.4.2. Kriging for a symmetrical problem

The interest of this section is to discuss the possibility of optimizing the kriging process by taking into consideration the physical properties of the problem. More specifically the symmetric properties for output results  $f^i(\mathbf{x}, \xi)$  and  $a^i(\mathbf{x}, \xi)$  with respect to  $k_v^{b,2} = k_h^{b,2}$  are discussed. To take this particularity in consideration, three different kriging strategies will be investigated:

- a classic strategy: a classic kriging is constructed with a chosen regression function  $\mathbf{g}$  and correlation function  $\mathcal{R}$ . For this first case the symmetric properties of output results are not used.
- a half-design space restriction strategy: as the problem is symmetric, a strategy where only using the points of the design space that satisfies  $k_v^{b,2} \leq k_h^{b,2}$  are used for the kriging construction is investigated. For the prediction, half of the design space is directly reconstructed by using the symmetric property.
- a symmetrical regression strategy: the symmetric aspect of the problem is introduced in the regression part directly. By this strategy, the “knowledge” of the physical problem is directly introduced in the meta-model. As an example, in dimension 2, if  $\mathbf{g}$  is the second order polynomial regression function for a classical kriging, the symmetric regression function  $\mathbf{g}_s$  would write:

$$\mathbf{g}_s(x_1, x_2) = \begin{cases} \beta_0 + \beta_1 x_1 + \beta_2 x_2 + \beta_3 x_1 x_2 + \beta_4 x_1^2 + \beta_5 x_2^2 & \text{if } x_1 \leq x_2 \\ \mathbf{g}_s(x_2, x_1) & \text{if } x_2 \leq x_1 \end{cases} \quad (12)$$

where  $x_1 = k_v^{b,2}$  and  $x_2 = k_h^{b,2}$ . This symmetry is then translated directly in the regression matrix.

### 3.5. Summary on the hybrid meta-modelling approach

As previously explained the mathematical formulation of the proposed hybrid meta-model is based on the combination of the PCE and the kriging meta-models. As a summary, the different functions (i.e. the critical speeds  $f^i(\mathbf{x}, \xi)$  and the associated amplitudes of vibration  $a^i(\mathbf{x}, \xi)$ ) to be estimated are approximated by:

$$\Gamma(\xi, \mathbf{x}) = \sum_{k=0}^{p-1} \gamma_k(\mathbf{x}) \Phi_{\alpha_k}(\xi) \quad (13)$$

It is worth emphasizing here that each critical speed  $f^i$  (each associated vibration amplitude  $a^i$ , resp.) have their own surrogate model that could be denoted  $\Gamma^{(f^i)}$  ( $\Gamma^{(a^i)}$ , resp.) For the sake of readability, the superscript is pulled out, but developments are done for each critical speed  $f^i$  and each associated vibration amplitude  $a^i$ . The random variable is approximated by a PCE whose coefficients depend on the parametric parameters  $\mathbf{x} = (k_h^{b,2}, k_v^{b,2})$ . Each PCE coefficient is then approximated by a kriging meta-model. It writes:

$$\gamma_k(\mathbf{x}) = \mathbf{g}^{(k)}(\mathbf{x})^T \boldsymbol{\beta}^{(k)} + Z^{(k)}(\mathbf{x}) \quad (14)$$

and finally:

$$\Gamma(\xi, \mathbf{x}) = \sum_{k=0}^{p-1} (\mathbf{g}^{(k)}(\mathbf{x})^T \boldsymbol{\beta}^{(k)} + Z^{(k)}(\mathbf{x})) \Phi_{\alpha_k}(\xi) \quad (15)$$

For the construction of the experimental designs, a set of  $Q$  points  $\mathbf{x}^{(k)}$  and a set of  $N$  points  $\xi^{(j)}$  are generated. The input points of the final experimental design are obtained by the tensorisation of these two sets and is composed of  $Q \times N$  points. For each  $(\mathbf{x}^{(k)}, \xi^{(j)})_{(k,j) \in [1,Q] \times [1,N]}$

the critical speeds  $f^i$  and the associated unbalance responses  $a^i$  are computed and taken as output values for the different experimental designs. So one gets  $N \times Q$  values of each critical speed  $f^i$  and of each vibration amplitudes  $a^i$ . This approach has the advantage to deal with two types of uncertain parameters (i.e. the two parametric parameters  $\mathbf{x} = (k_h^{b,2}, k_v^{b,2})$  and the seven random parameters  $\xi = [\xi_E, \xi_{e_1}, \xi_{e_2}, \xi_{e_3}, \xi_{e_4}, \xi_{k_h^{b,1}}, \xi_{k_v^{b,1}}]$  in the present case). The general workflow is illustrated in Fig. 3. The second advantage is the direct access to stochastic properties as explained in the next part.

### 3.6. Exploitation of the PCE

From the PCE, exploiting the coefficients  $\gamma_k$  gives a direct access to the statistical moments of the outputs (mean and variance). From the previous formulation, it means the statistical moments are directly an analytical function of the parametric parameters (Blatman and Sudret, 2011; Sudret, 2008).

From the PCE, the average of  $\Gamma$  at the point  $\mathbf{x}$  is then equal to:

$$\mathbb{E}[\Gamma(\mathbf{x})] = \gamma_0(\mathbf{x}) = \mathbf{g}^{(0)}(\mathbf{x})^T \boldsymbol{\beta}^{(0)} + Z^{(0)}(\mathbf{x}) \quad (16)$$

and for the variance, it comes:

$$\sigma_{\Gamma(\mathbf{x})}^2 = \sum_{k=1}^{p-1} \gamma_k(\mathbf{x})^2 \|\Phi_{\alpha_k}\|^2 = \sum_{k=1}^{p-1} (\mathbf{g}^{(k)}(\mathbf{x})^T \boldsymbol{\beta}^{(k)} + Z^{(k)}(\mathbf{x}))^2 \|\Phi_{\alpha_k}\|^2 \quad (17)$$

Hence the statistical moments are obtained directly from the kriging meta-model, with an almost null numerical cost. It is worth emphasizing here that if a unique kriging meta-model were created for all the parameters, at this step it would have been necessary to perform a Monte Carlo Simulation (MCS) on the kriging meta-model to estimate the mean and variance, representing a non-negligible computational time.

The Sobol indices can also be directly deduced from the PCE coefficients due to the uniqueness of the decomposition (Sudret, 2008). Let  $V(\Gamma(\mathbf{x}))$  be the variance of the output  $\Gamma$  at the point  $\mathbf{x}$  of the parametric space. The first order Sobol index  $S_i(\mathbf{x})$  related to the variable  $i \in [E, e_1, e_2, e_3, e_4, k_h^{b,1}, k_v^{b,1}]$  is equal to (Sobol, 1993):

$$S_i(\mathbf{x}) = \frac{V_i(\mathbf{x})}{V(\Gamma(\mathbf{x}))} \quad (18)$$

where  $V_i(\mathbf{x}) = V(\mathbb{E}(\Gamma(\mathbf{x}))|X_i)$  is obtained directly from the PCE coefficients:

$$V_i(\mathbf{x}) = \sum_{k \in \alpha_i} \gamma_k(\mathbf{x})^2 \|\Phi_{\alpha_k}\|^2 \quad (19)$$

where  $\alpha_i$  is the set of multivariate indices for which only polynomials related to the variable  $i$  are present (i.e.  $\alpha_i > 0$  and  $\alpha_j = 0$  for  $j \neq i$  and  $i \in [E, e_1, e_2, e_3, e_4, k_h^{b,1}, k_v^{b,1}]$ ).

## 4. Application on the rotor system

This section is devoted to discuss the efficiency of the proposed hybrid meta-modelling approaches for the prediction of the critical speeds  $f^i$  and the associated amplitudes  $a^i$  of the rotor system under study. Firstly, a brief discussion on the data generation as well as the PCE and kriging constructions is proposed. Then results of the three hybrid meta-modelling approaches are compared and the variance-based sensitivity analysis based on Sobol indices is performed.

### 4.1. Preamble on the use of hybrid meta-models

#### 4.1.1. Data generation: experimental designs and validation sets

As previously explained, two sets are constructed for the experimental design creation: one for the PCE and one for the kriging meta-model. For the PCE, the input points are generated with a Latin Hypercube Sampling (LHS) of  $N = 250$  points (i.e. 250 values of  $\xi$ ). For the kriging, the input points are generated with a maximin LHS of  $Q$  points to

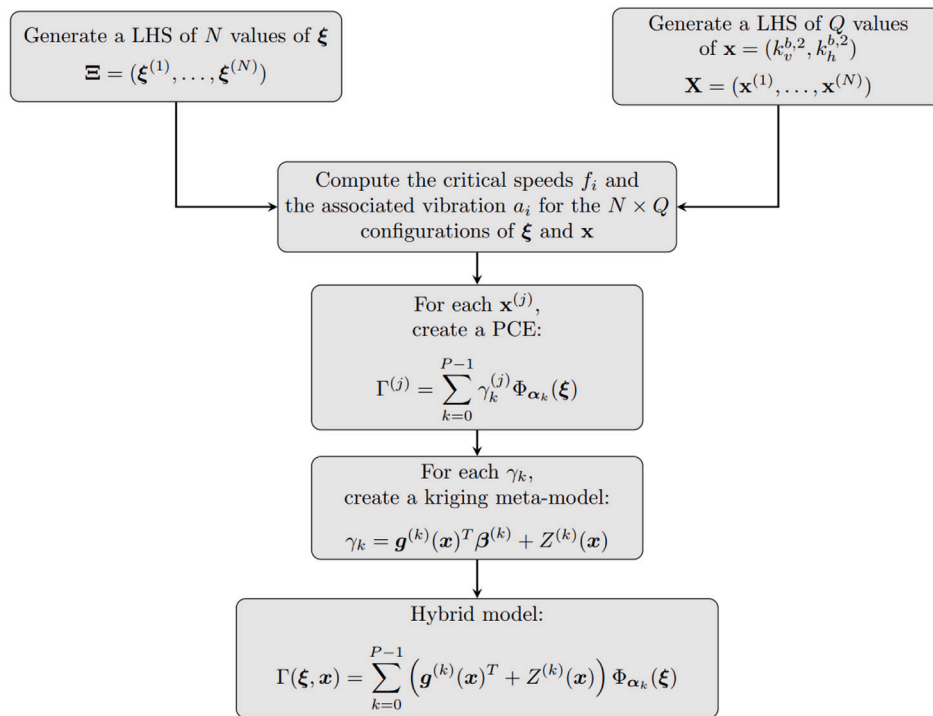


Fig. 3. General workflow of the method.

ensure an homogeneous distribution of the points over the input space. To compare the performances of the different kriging meta-models, four different sizes are considered here, namely 20 points, 40 points, 60 points and 80 points. The model is evaluated for all the combinations, i.e. for the  $N \times Q$  cases.

To validate the different meta-models, two different validation steps are performed:

- validation of the PCE: for this, for eight of the  $\mathbf{x}$  values, an LHS of 500 points of  $\xi$  has been generated for comparison to validate each PCE. With this, the PCE predictions at some specific locations  $\mathbf{x}$  in the design space are compared to reference values. This set aims at tuning the PCE properties (chaos order and hyperbolic norm) and validating the different PCE and ensure their properties are valid over the full design space.
- validation of the final hybrid meta-models: for this, a regular grid of  $100 \times 100$  couples  $(k_v^{b,2}, k_h^{b,2})$  is generated. For each point, the average and the variance of the eight critical speeds  $f^i$  and the eight associated vibration amplitudes  $a^i$  are obtained by performing a MCS with 1000 values of  $\xi$ . The evaluation of the final meta-model is then performed by comparing these reference averages and variances to the ones predicted by the different meta-models. This set aims at validating the full hybrid surrogate model on the whole space.

#### 4.1.2. PCE construction

The different PCE are first constructed for each case, i.e. for each critical speed  $f_i$  and each associated maximum of vibration amplitude  $a_i$  and for each value of the  $Q$  values  $\mathbf{x}$ . The parameters to be determined are the chaos order  $m$  and the hyperbolic norm  $q$ . The polynomial basis is chosen to be the same over the parametric space for one critical speed or one associated vibration amplitude. The choice of  $m$  and  $q$  is made to minimize the prediction error between the PCE predictions and the reference results using the sets of 500 points for different values of  $\mathbf{x}$ . The final choice of parameters is summarized in Table 6.

Two tendencies emerge. First, higher chaos order are required for the first modes which demonstrates more complex coupling effects

between the different parameters for these modes than for the higher frequency modes. Second, higher chaos order are required for the maximum of vibration amplitude than for the critical speeds.

#### 4.1.3. Kriging construction

Once the different PCE have been constructed for each point of the parametric experimental design, one kriging meta-model is constructed for each PCE coefficient. As a reminder, twelve cases are investigated here: four different experimental design sizes and three different kriging strategies. The kriging properties (regression and correlation functions) are the same for one PCE coefficient to keep consistency for comparison. The choice of the optimal parameters was done for the experimental design of 60 points and a classic kriging strategy. It appears that keeping the same kriging properties for all the critical speeds PCE coefficients was a good strategy. For the maximum amplitude of

Table 6  
PCE characteristics for the different cases.

Mode number	Quantity	Chaos order $m$	$q$ value	Total number of terms
1	Critical speed	3	0.7	43
	Max. ampl	6	0.4	64
2	Critical speed	3	0.7	43
	Max. ampl	10	0.3	71
3	Critical speed	3	0.7	43
	Max. ampl	6	0.4	64
4	Critical speed	3	0.7	43
	Max. ampl	3	0.7	43
5	Critical speed	2	0.4	15
	Max. ampl	8	0.4	71
6	Critical speed	2	0.4	15
	Max. ampl	3	0.7	43
7	Critical speed	2	0.4	15
	Max. ampl	3	0.7	43
8	Critical speed	2	0.4	15
	Max. ampl	3	0.7	43

**Table 7**  
Kriging correlation functions for the different cases.

Mode number	Quantity	Correlation function
1	Critical speed	Linear
	Max. ampl. — 1st term	Spline
	Max. ampl. — other terms	Spherical
2	Critical speed	Linear
	Max. ampl. — 1st term	Linear
	Max. ampl. — other terms	Spherical
3	Critical speed	Linear
	Max. ampl. — 1st term	Linear
	Max. ampl. — other terms	Spherical
4	Critical speed	Linear
	Max. ampl. — 1st term	Linear
	Max. ampl. — other terms	Spherical
5	Critical speed	Linear
	Max. ampl. — 1st term	Matérn 5/2
	Max. ampl. — other terms	Linear
6	Critical speed	Linear
	Max. ampl. — 1st term	Linear
	Max. ampl. — other terms	Linear
7	Critical speed	Linear
	Max. ampl. — 1st term	Matérn 5/2
	Max. ampl. — other terms	Linear
8	Critical speed	Linear
	Max. ampl. — 1st term	Linear
	Max. ampl. — other terms	Linear

vibrations at each critical speed, the correlation for the first PCE term (related to the mean) can sometimes be different than for the others (related to the variance). Finally, a second order polynomial regression was chosen here. The correlation functions for the different cases are summarized in Table 7.

#### 4.2. Comparison of the three different kriging strategies

The different kriging construction strategies previously defined in Section 3.4.2 are then compared. To do so, the second validation set is used, it consists of a regular grid of  $100 \times 100$  couples  $\mathbf{x} = (k_v^{b,2}, k_h^{b,2})$ . For each of these points, the critical speeds  $f^i(\mathbf{x}, \xi)$  and the associated vibration amplitudes  $a^i(\mathbf{x}, \xi)$  are computed for a MCS of 1000 points to take into consideration the seven random uncertainties  $\xi = [\xi_E, \xi_{e_1}, \xi_{e_2}, \xi_{e_3}, \xi_{e_4}, \xi_{k_h^{b,1}}, \xi_{k_v^{b,1}}]$ . The average and the variance are then deduced. The kriging predictions of the mean and variance (directly deduced from the PCE coefficients from Eqs. (16) and (17)) are compared to the reference values. The average and variance of the relative error over the grid is computed. This error is defined as:

$$Error(\mathbf{x}) = \frac{r_p(\mathbf{x}) - r_{ref}(\mathbf{x})}{|r_{ref}(\mathbf{x})|} \quad (20)$$

where  $r_p(\mathbf{x})$  and  $r_{ref}(\mathbf{x})$  defines the prediction result and the reference solution, respectively. This relative error is computed for the eight critical speeds ( $f^i$ ) and for the eight associated vibration amplitudes ( $a^i$ ) and for all the difference cases: the three kriging strategies discussed in Section 3.4.2 are tested for four different Experimental Design (ED) patterns (i.e. for a number of 20, 40, 60 and 80 samples respectively). The means and variances of the relative errors over the grid for the critical speeds of the first eight modes (i.e. the first four backward and forward modes) are given in Figs. 4 and 5, respectively. The means and variances of the associated amplitudes of vibration are also given in Figs. 6 and 7, respectively.

Looking at the estimation of the critical speeds, one can observe these different points:

- the errors are always very low as both the mean and the variance of the latter are extremely low (around  $8.10^{-1}$  in the worst case). This illustrates the good approximation given by the proposed strategy in all cases.

- increasing the ED size tends to decrease the error until the convergence is reached. The convergence is globally reached more quickly for higher modes than for the first modes (see Figs. 4(a) and 5). In most cases, the convergence is reached quickly with only 40 points, which illustrates the fact that a small number of samples is sufficient to accurately predict the outputs of interest.
- the error is globally higher for the first modes than for the last ones (see for example the low error on modes 5 to 8 in Fig. 4(a)). The evolutions of the frequencies mean and variance are indeed more complex for these first four modes which makes the prediction more difficult for the same level of information. This fact this will be illustrated later and discussed in detail in the paper.
- comparing the different kriging strategies for the last four modes, the low level of error (lower than  $10^{-3}$  in average and lower than  $10^{-7}$  in variance) makes the comparison worthless between the different strategies as they are all performing well.
- comparing the different kriging strategies for the first four modes, depending on the case, the half-design space restriction strategy or the symmetrical regression strategy performs better. For the mean frequency, the symmetric regression kriging has better performances and sometimes represent a considerable improvement. For example, to estimate the average of the fourth critical speeds (see Fig. 4(a)), a symmetric regression kriging divides by two the error. But if one considers the estimation of the frequency variance, the half-design spaces strategy performs better for the first modes.

As a conclusion, the three kriging strategies perform well. However, in some cases the symmetric regression kriging and the half-design spaces kriging performs a bit better and so could be used preferably to the classical kriging. Moreover, it is worth emphasizing here that the half-design spaces strategy requires twice less points than the two other kriging strategies and so has to be preferably chosen as it presents the best ratio between the prediction quality and the numerical cost. These results clearly illustrate the interest of taking into account known properties of symmetries on the physical output results.

For the maximum amplitudes estimation at the first eight critical speeds, the following comments can be drawn from Figs. 6 and 7:

- the level of error varies a lot from one mode to another, and the errors tend to be lower for the forward modes (even number) than for the backward modes (odd number), especially for the average mean amplitude estimation. This can easily be explained by the fact that the amplitudes of the backward modes are almost zero when considering the case of equal stiffnesses  $k_v^{b,2} = k_h^{b,2}$ . Also, this naturally leads to a higher error estimate in the presence of uncertainties, because the latter lead to non-negligible relative amplitude variations.
- increasing the ED size tends to reduce the error in average and variance. The error converges more or less quickly depending on the case.
- the error is larger for the amplitude of the backward modes than those of the forward modes. This is explained by the fact that when one considers equal stiffnesses  $k_v^{b,2} = k_h^{b,2}$  for the second bearing support (i.e. symmetric rotor if there is no random parameters), the vibration amplitudes drop brutally to almost zero. Thus, a small error for this case would represent a high relative variation, and would lead to a high error. This is not observed for the critical speeds, as their evolutions are more continuous and smoothed with numerical values that remain always far from zero. Consequently the relative errors are then much lower, even in the case of  $k_v^{b,2} = k_h^{b,2}$ , as they are balanced by a large non zero value.
- globally, the classical kriging is the worst strategy and the half-design strategy performs better than the others. Nevertheless, it is worth emphasizing here that for the 20 points case, the symmetric

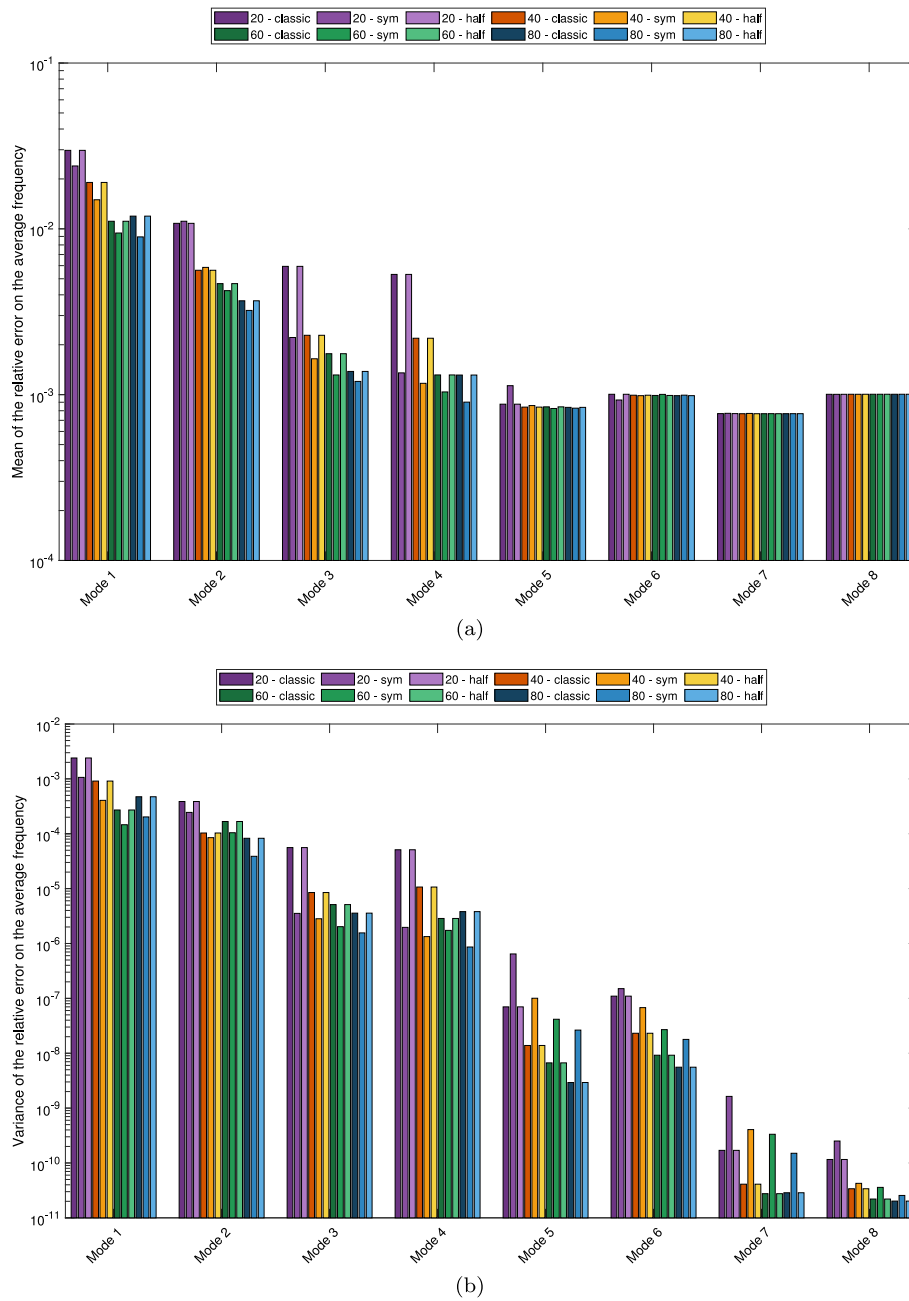


Fig. 4. Average (a) and variance (b) of the relative error on the mean for the critical speeds of the first eight modes (i.e. the first four backward and forward modes).

strategy performs better than the others. And using 20 points with a symmetric regression leads to better results than using 80 points with a classic kriging strategy, illustrating the drastic numerical cost reduction such strategy can bring (see for example the mode 5 in Figs. 6 and 7). For larger sets, using symmetric or a half-design space kriging strategies gives better results with 40 learning points (about 20 points for the half-design spaces kriging as half of the ED is removed) than a classical kriging with 80 learning points (see Figs. 6 and 7 for modes 3, 5, 6 and 8). This gives a drastic reduction of the required number of learning points and an improvement of the prediction results.

From these observations and as previously stated for the estimation of the critical speeds, it comes that adding information about the problem symmetry in the kriging construction improves drastically its prediction quality and allows to reduce the number of required learning points.

Comparing the different results, the best kriging strategy is the half-design space strategy as it performs better in many cases, and requires twice less learning points.

As a complementary illustration of the results, the reference results and the half-design kriging predictions are displayed for comparison in Fig. 8 for the frequencies of the critical speeds and in Fig. 9 for the associated maximum amplitudes. Only the first six modes are given for the sake of concision. These predictions are obtained for the 60 points experimental design and with the half-design strategy as it was stated it was the best strategy. The 3D surfaces represents the average of the critical speeds  $f^i$  (resp. the amplitudes  $a^i$ ) and the average  $\pm$  the standard deviation are in red and blue. In order to better illustrate and comment on the results obtained, a cross-sectional view along the two main diagonals of the experimental design is provided (from  $(k_v^{b,2}, k_h^{b,2}) = [0.1, 0.1] 10^6$  to  $[2, 2] 10^6$  N/m with  $k_v^{b,2} = k_h^{b,2}$  for the first cross-section and from  $(k_v^{b,2}, k_h^{b,2}) = [0.1, 2] 10^6$  to  $[2, 0.1] 10^6$  N/m

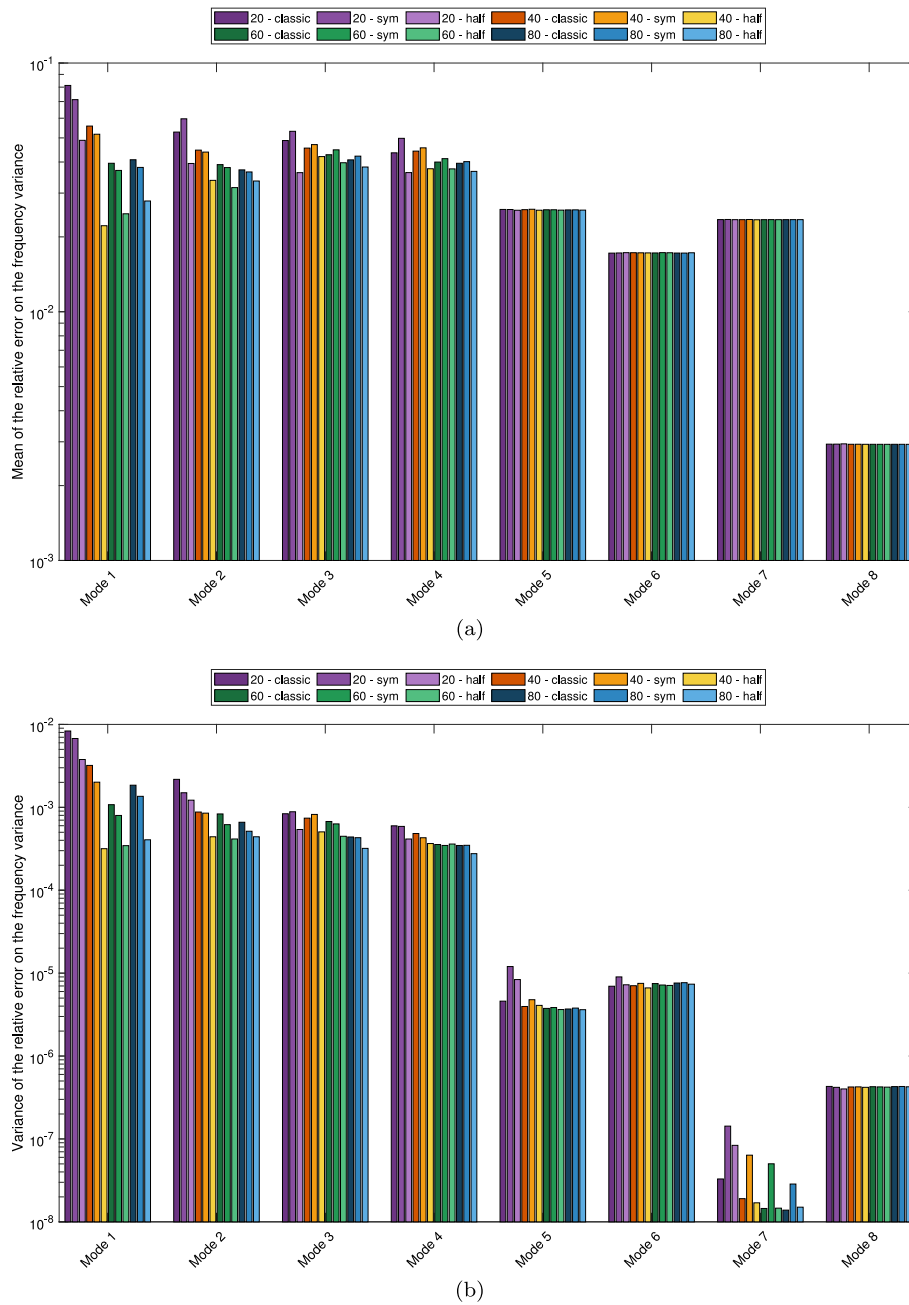


Fig. 5. Average (a) and variance (b) of the relative error on the variance for the critical speeds of the first eight modes (i.e. the first four backward and forward modes).

with  $k_v^{b,2} + k_h^{b,2} = 2.1 \cdot 10^6$  N/m for the second cross-section). The predictions on these two diagonals are given on the two right columns for the reference case (in black) and the three kriging strategies. This visualization has the advantage to give better insights in the kriging performances and their differences.

Considering the frequencies prediction in Fig. 8, the different kriging predictions are all visually very good, and differences between the two surfaces for each mode are barely visible. Even looking at the predictions at the two predefined diagonal cross sections, one can observe that the different kriging strategies perform well and no large differences are observable. The difference between the different kriging strategies is nevertheless well illustrated on some cases. Indeed, looking at the second diagonal cross section (last column in Fig. 8) for the modes 2, 3 and 4, one can see that the symmetric and the half-design strategies enable the presence of a singularity (non derivability) at  $k_v^{b,2} = k_h^{b,2}$ , which is not the case for the classic kriging strategy. As the

frequencies of the critical speeds have a smooth evolution, this property does not bring a large improvement in terms of prediction here.

Looking at the amplitudes prediction in Fig. 9, one can see that the shapes of the functions are more complex than for the frequencies. One can see the sharp evolutions of the vibration amplitudes around the symmetric axis (i.e. the first diagonal cross section defined by  $k_v^{b,2} = k_h^{b,2}$ ) and the drop to almost 0 amplitude for backward modes. Consequently more learning points are required to be able to catch this sharp evolution of the variation of the mean amplitude around this specific case. As previously explained, the fact that the vibration amplitudes are close to 0 at the first diagonal cross section can lead to significant error estimate in the presence of uncertainties. This is only due to the fact that uncertainties lead to non-negligible relative amplitude variations. Despite this, the kriging remains efficient and the level of prediction satisfactory, except for the first mode where the behaviour on the diagonal  $k_v^{b,2} = k_h^{b,2}$  is not caught for low stiffness

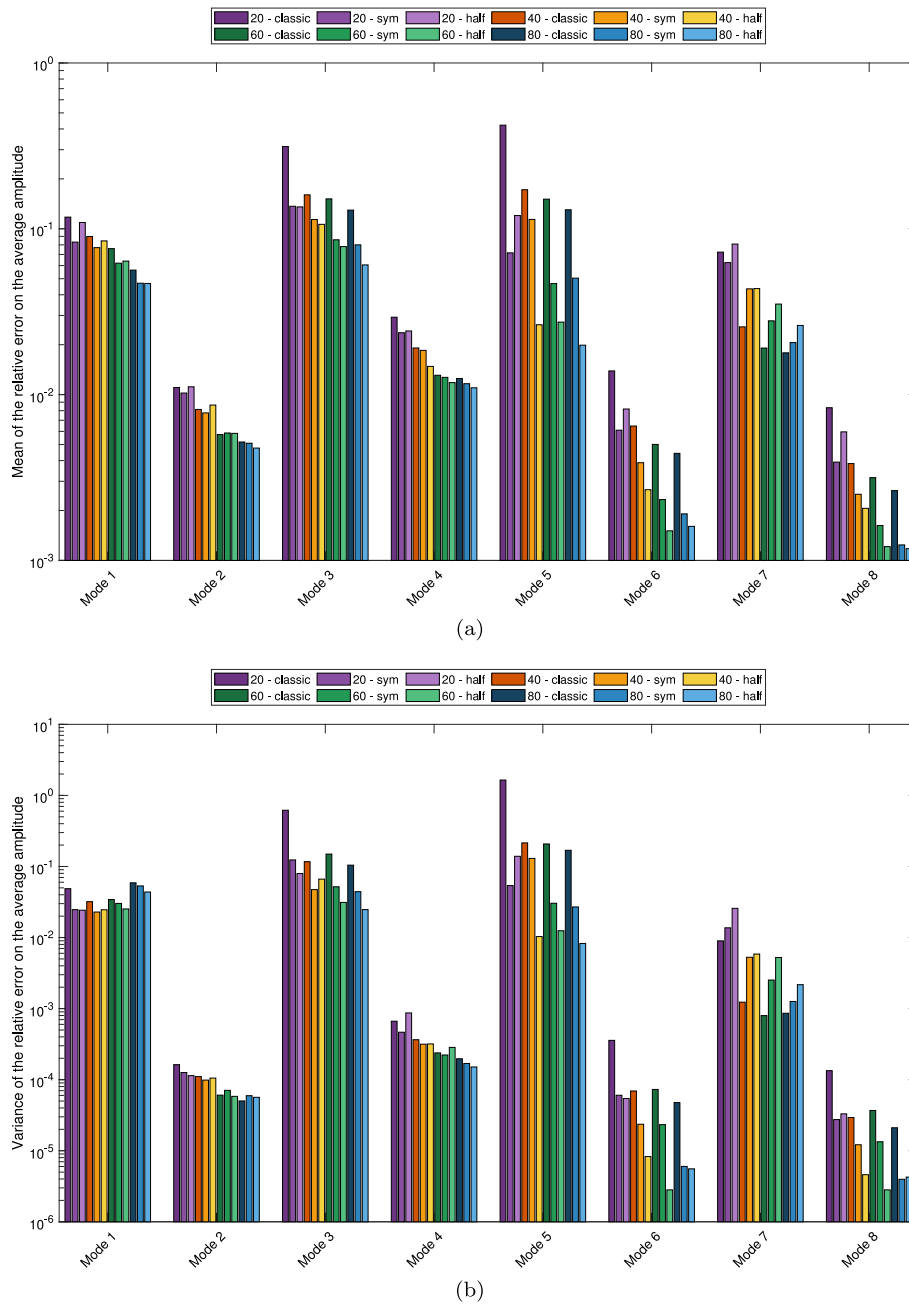


Fig. 6. Average (a) and variance (b) of the relative error on the mean of maximum amplitude at the first eight critical speeds (i.e. the first four backward and forward modes).

values. Looking at the predictions on the two diagonal cross sections (two last columns in Fig. 9, the differences between the different kriging strategies are more clear. First, the differences between the three kriging strategies are observable only around the case  $k_v^{b,2} = k_h^{b,2}$  (see last column in Fig. 9 for stiffness values far from the middle, close to  $k_v^{b,2} = 1 \cdot 10^6$  N/m). Globally, the half-design kriging performs better than the two other strategies as it gives better results around the case  $k_v^{b,2} = k_h^{b,2}$  (see modes 1, 3, 5 and 6). Comparing the symmetric case to the classical case, one can see that in some cases they perform similarly (see mode 2), illustrating that the random part of the kriging prevails on the regressive part. But in other cases, the symmetric case enable to catch more efficiently the evolution at  $k_v^{b,2} = k_h^{b,2}$  (see modes 1, 3, 5 and 6).

Similarly to the analysis of the errors, these results illustrate that adding information about the problem symmetry in the kriging construction enables to increase the prediction quality. As previously, the

best kriging strategy is the half-design space as it is the strategy that catches the most efficiently the parameter variations around the case  $k_v^{b,2} = k_h^{b,2}$ .

#### 4.3. Variance-based sensitivity analysis based on Sobol indices

Now a sensitivity analysis based on the Sobol method is discussed. The Sobol indices can be deduced directly from the PCE coefficients without any additional numerical cost, and so are directly predictable from the kriging meta-models. As previously, the kriging based on the half-design space strategy is employed as it has been demonstrated it has the best performances. First (total, respectively) order Sobol indices are given in Fig. 10 (Fig. 11, respectively) for the frequencies of the critical speeds and in Fig. 12 (Fig. 13, respectively)) for the maximum of amplitude. As a reminder, Sobol indices are indicators that enable to state on the contribution of one input on the output variance. Thus,

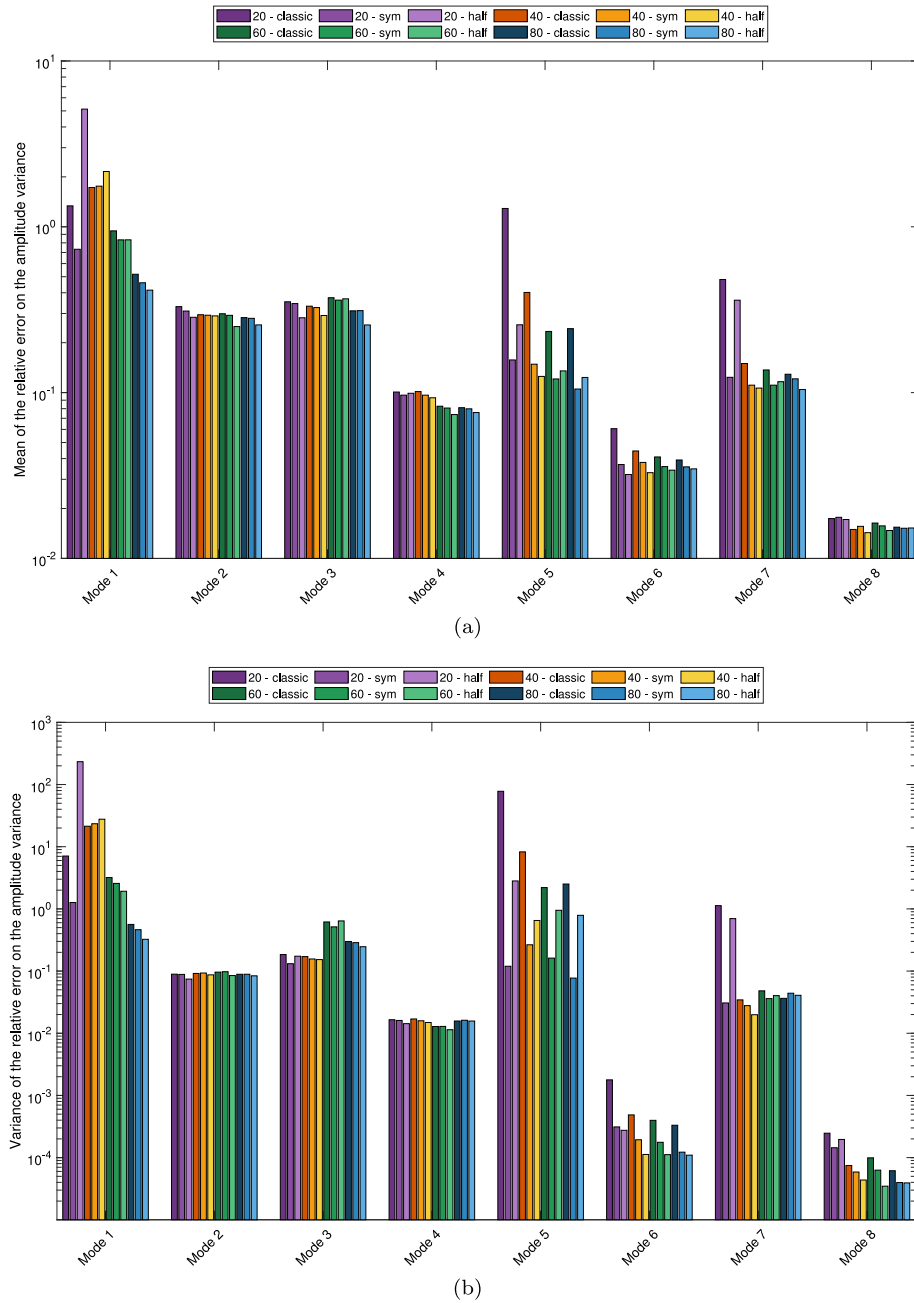


Fig. 7. Average (a) and variance (b) of the relative error on the variance of maximum amplitude at the first eight critical speeds (i.e. the first four backward and forward modes).

if the Sobol index of a parameter  $i$ , denoted  $S_i$ , is near 1, then this parameter has a high influence on the output, whereas if  $S_i$  is near 0 then this parameter has almost no influence. First order Sobol index refers to the contribution of one parameter alone, whereas the total Sobol index refers to all its contribution by taking into account the coupling with the other parameters.

Considering the Sobol indices of the frequencies in Figs. 10 and 11, one can clearly see that the behaviour of the different Sobol indices are completely different from a parameter to another and from a mode to another. First, the main influential parameters depend on the considered mode. For example, the thickness of the first disc  $e_1$  has a large influence on the critical speed of the modes 1, 2, 3, 4, 5 and 7, but has almost no influence for modes 6 and 8. This result is of course directly related to the influence of added masses and gyroscopic effects at disc 1 on the different modes. Second, the influence of one parameter depends strongly on the values of  $k_v^{b,2}$  and  $k_h^{b,2}$ . For example,  $S_E$  reaches

its maximum for large values of both stiffnesses  $k_v^{b,2}$  and  $k_h^{b,2}$  for the modes 1 to 4, whereas it corresponds to its minimum for higher modes. By comparing the first order and total order Sobol indices, it comes that almost no coupling effect exist between the parameters as the total indices are equal to the first order indices. Finally, the evolution of the Sobol indices of the first modes is more complex than the evolution of the last four modes. In spite of all these variations, a few general observations can be done for each mode:

- mode 1: for low stiffness values, the thicknesses of the discs 3 and 4 are the main parameters, whereas for higher values contributions are shared between the Young modulus of the shaft  $E$ , the thickness of the first disc  $e_1$  and the vertical stiffness of the first bearing  $k_v^{b,1}$ .
- mode 2: except at very low stiffness values, the main parameters are the shaft Young modulus  $E$ , the thickness of the first disc  $e_1$  and the horizontal stiffness  $k_h^{b,1}$ . At very low stiffness values

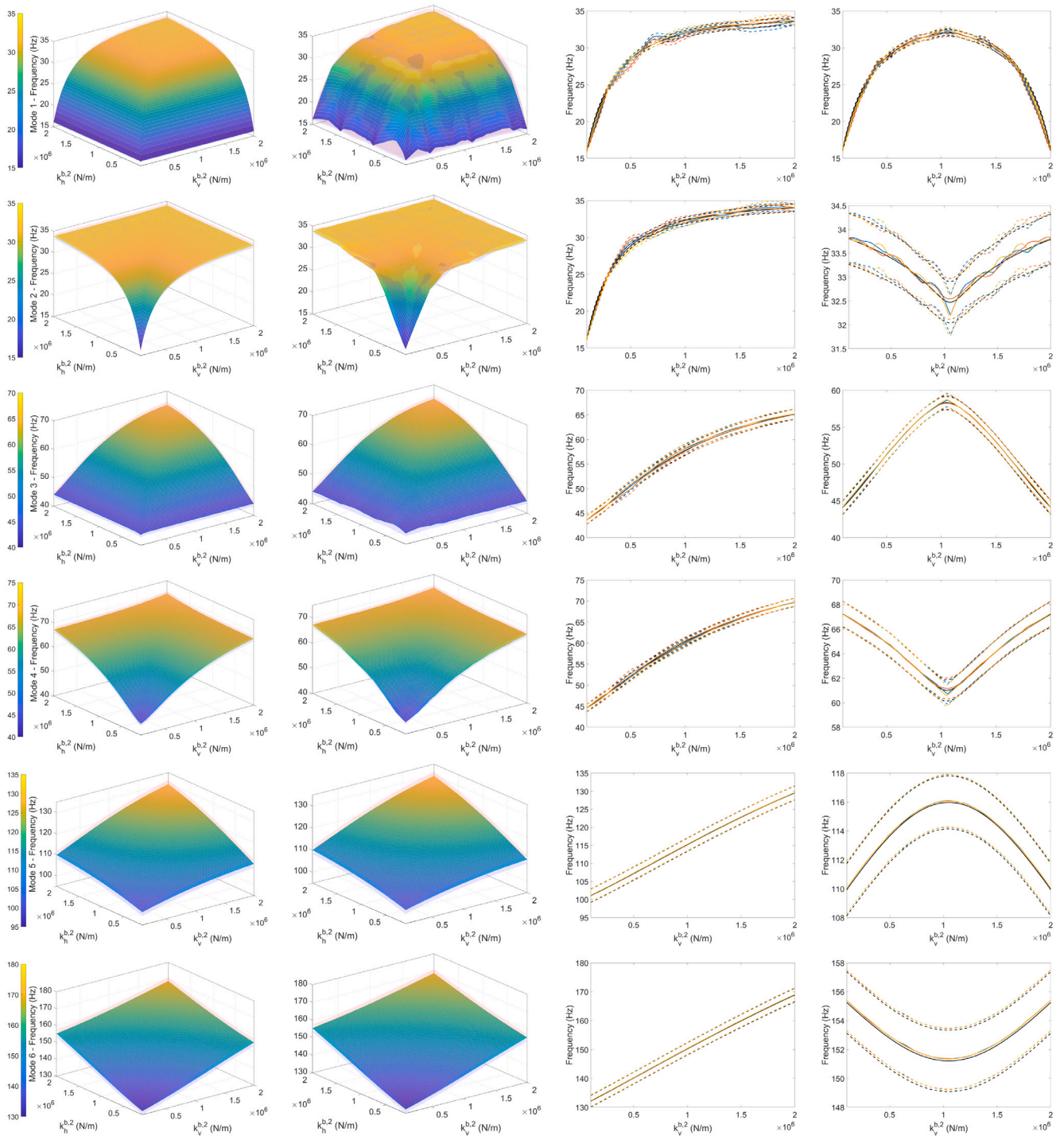


**Fig. 8.** Evolution of the average, average  $\pm$  standard deviation of the frequency for the reference (first column), half-design kriging (second column) — Zoom on the diagonal  $k_v^{b,2} = k_h^{b,2}$  (third column) and on the diagonal  $k_v^{b,2} + k_h^{b,2} = 2.1 \cdot 10^6$  N/m (last column): full line = average, dotted line = average  $\pm$  standard deviation, black = reference, orange = classic, blue = symmetric kriging, yellow = half-design. (For interpretation of the references to colour in this figure legend, the reader is referred to the web version of this article.)

(inferior to about  $0.12 \cdot 10^6$  N/m), the thicknesses of the discs 3 and 4 are the main parameters. The switch between the main influential parameters (and so the evolution of the Sobol indices) is similar to the evolution of the corresponding frequency (see in Fig. 8 the jump in frequency from 15 Hz and 35 Hz).

- mode 3: the thickness of the first disc  $e_1$  remains the parameter with the highest influence on the critical speed (see  $S_{e_1}$  always between 0.66 and 0.78). Then, four parameters have alternatively

a moderate influence, namely  $e_3$ ,  $e_4$  and  $k_v^{b,1}$ . One can notice their areas of influence do not overlap. The contribution of the remaining parameters is always somewhat negligible.

- mode 4: the thickness of the first disc  $e_1$  is the parameter with the highest influence, contributions of  $e_3$ ,  $e_4$  and  $k_h^{b,1}$  are observed. As for the mode 2, the increase in the critical speed is correlated to the decrease of  $S_{e_1}$  and in the increase of the Sobol indices of the other parameters.

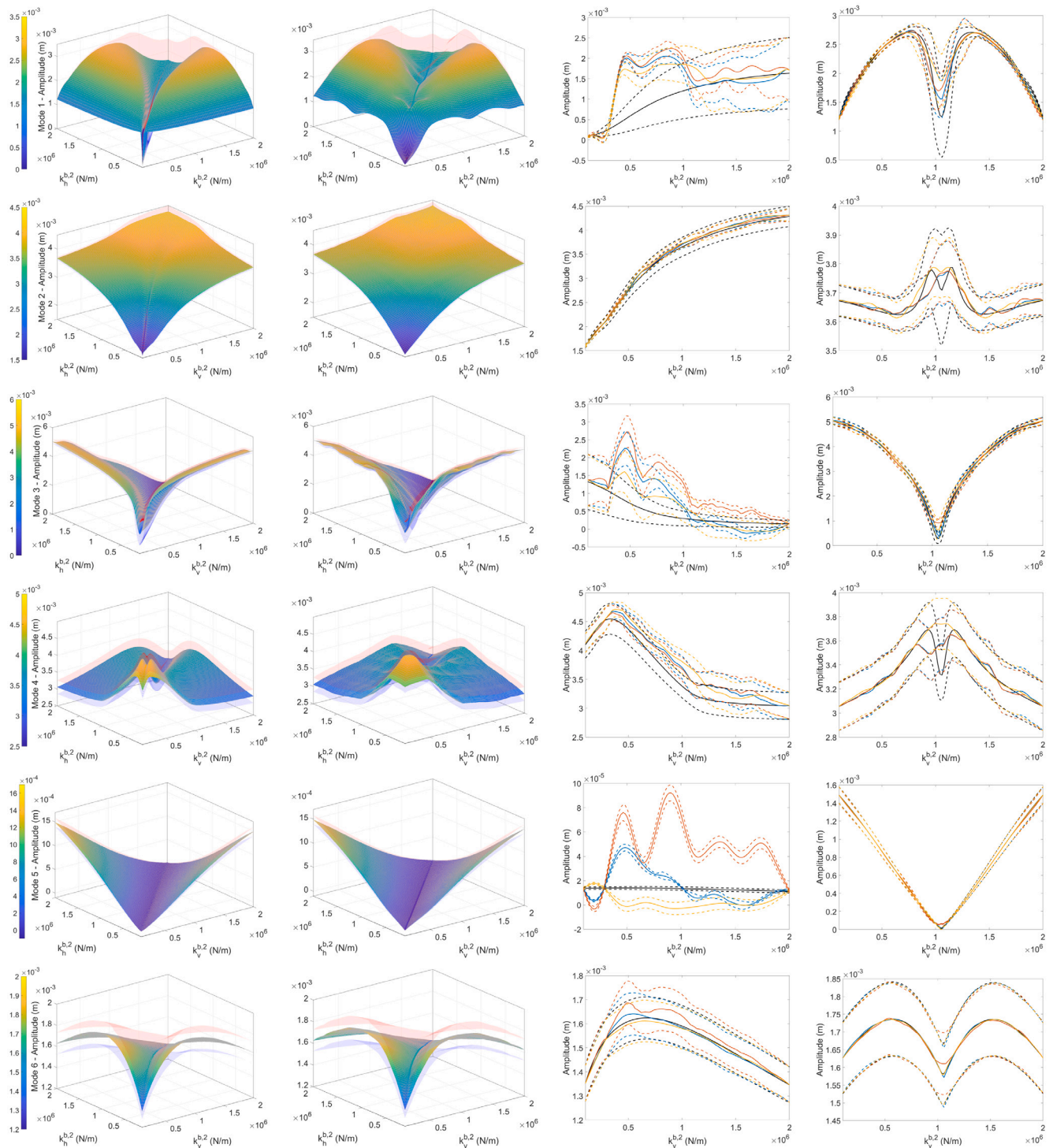


**Fig. 9.** Evolution of the average, average  $\pm$  standard deviation of the maximum amplitude for the reference (first column), half-design kriging (second column) — Zoom on the diagonal  $k_v^{b,2} = k_h^{b,2}$  (third column) and on the diagonal  $k_v^{b,2} + k_h^{b,2} = 2.1 \cdot 10^6$  N/m (last column): full line = average, dotted line = average  $\pm$  standard deviation, black = reference, orange = classic, blue = symmetric kriging, yellow = half-design. (For interpretation of the references to colour in this figure legend, the reader is referred to the web version of this article.)

- mode 5: the thickness of the first disc  $e_1$  and the Young modulus  $E$  are the two most influential parameters with similar Sobol indices values between 0.3 and 0.45. For high stiffnesses values of  $k_v^{b,2}$  and  $k_h^{b,2}$ ,  $e_4$  has also a non-negligible contribution but of second order.
- mode 6: the Young modulus  $E$  always has an important contribution (see  $S_E$  between 0.3 and 0.7), but is preponderant for low stiffnesses values of  $k_v^{b,2}$  and  $k_h^{b,2}$ . For larger values of the latter,

- the critical speed is also largely influenced by the thicknesses of the second and fourth discs  $e_2$  and  $e_4$ , respectively.
- mode 7: the critical speed is mostly influenced by the shaft Young modulus and the thickness of the first disc.
- mode 8: the critical speed is mostly influenced by the shaft Young modulus, and then by the thickness of the second and third discs  $e_2$  and  $e_3$ .

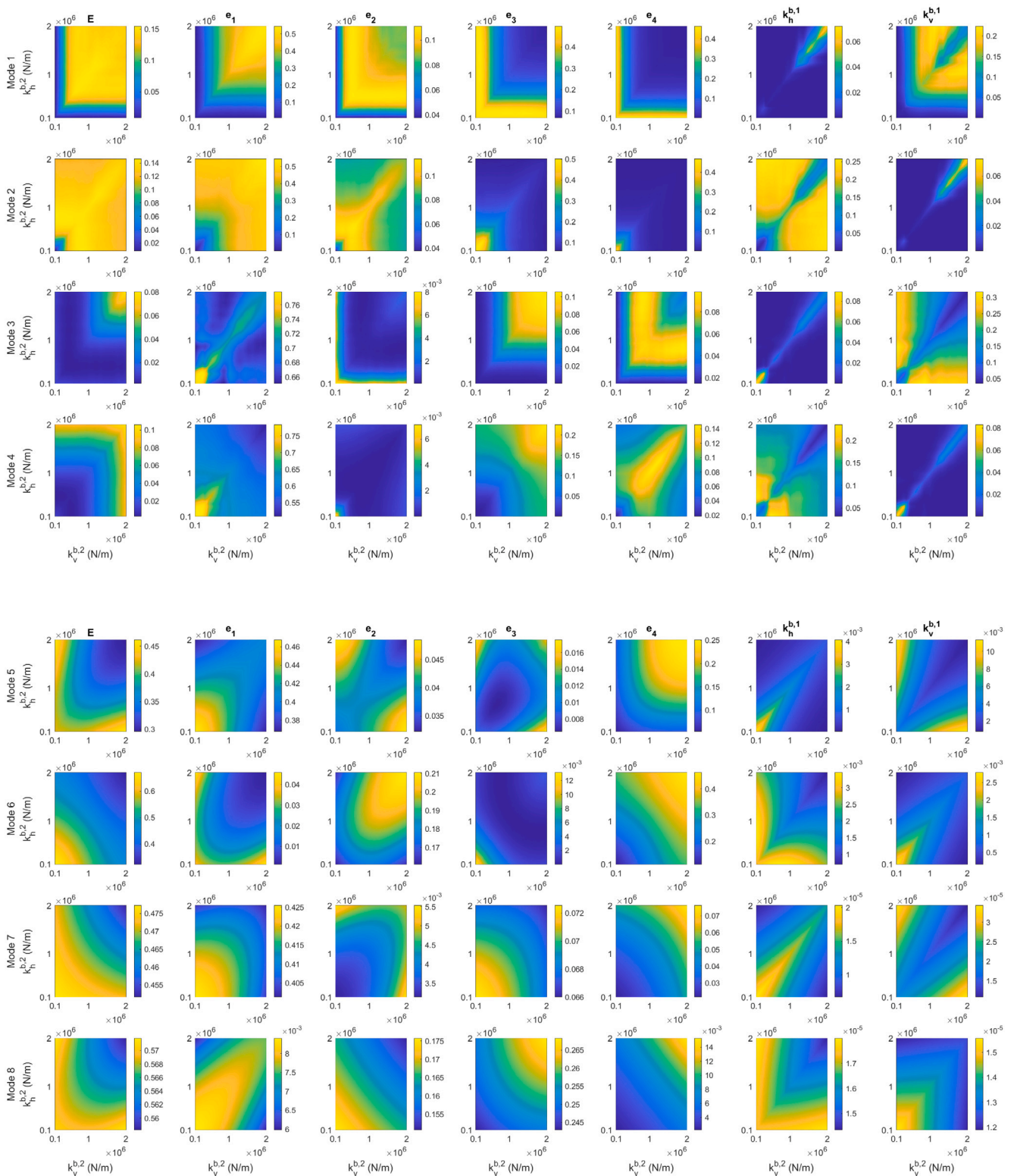


Fig. 10. First order Sobol indices of the modes 1 to 8 — Critical speeds.

It is worth noticing that the influence of the disc thickness parameters  $e_i$  (for  $i = 1, \dots, 4$ ) are different for each mode and are directly related to the positioning of each disc on the rotor system. Indeed, if a disc is located close to a node of vibration (at one maximum amplitude between two nodes for a specific mode shape, respectively) adding mass due to a thickness variation of the disc leads to negligible (predominant respectively) effects on the structural dynamic behaviour of the rotor

system. Likewise the gyroscopic effects will be predominant when the derivative of the mode deflection is maximal (and negligible when the latter is null). This explains the complexity and diversity of the results obtained for each mode according to the variations in thickness of the different discs.

Considering the Sobol indices of the associated vibration amplitudes in Fig. 12, one can see that the evolution of the Sobol indices is even

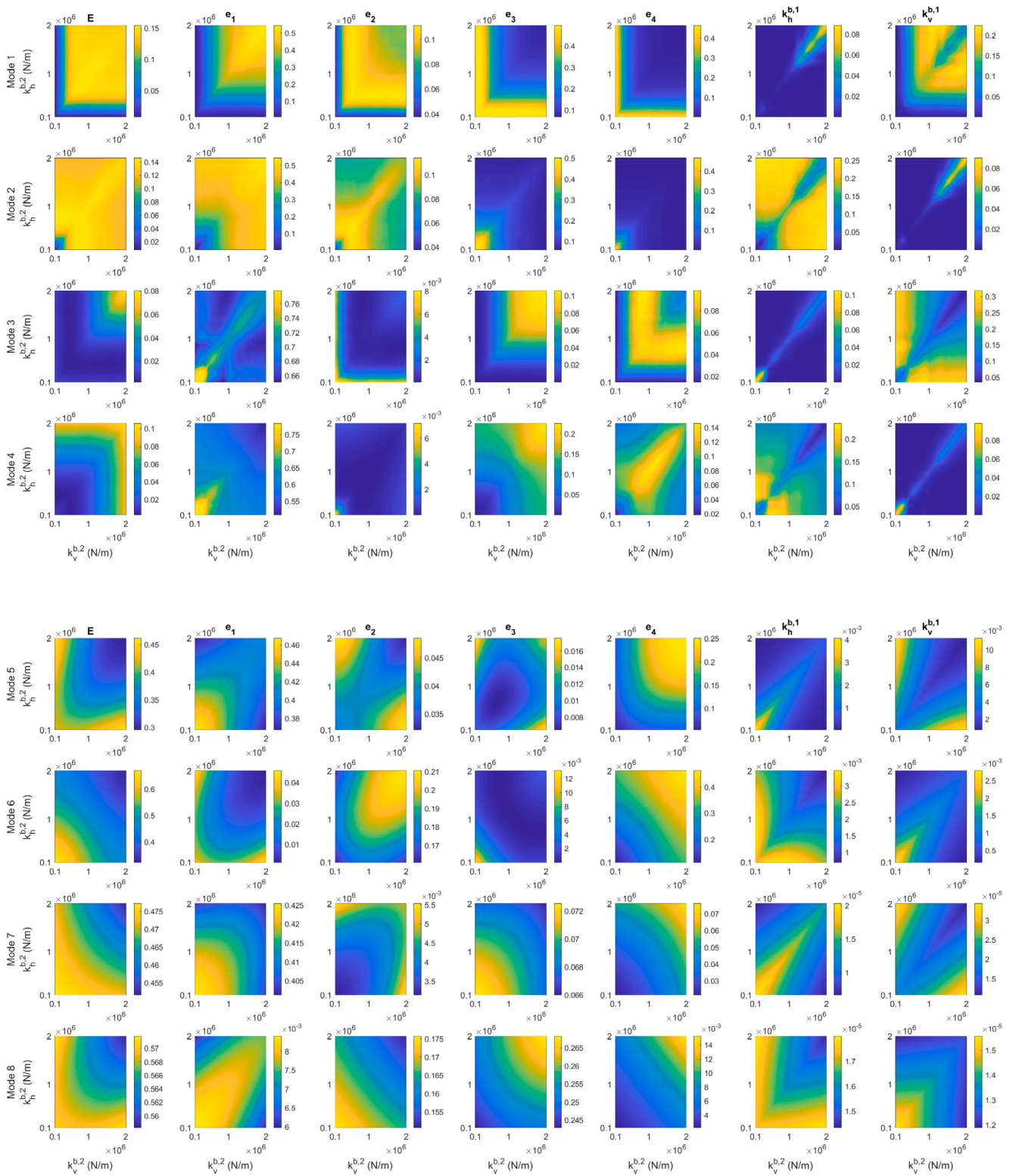


Fig. 11. Total order Sobol indices of the modes 1 to 8 — Critical speeds.

more complex with some very localized contribution (see  $S_{e_3}$  for mode 1). Moreover, the symmetry axis is more visible than for the critical speeds, which means that depending on the symmetrical properties of

the rotor, the influential parameters change. As for the frequencies, the contribution of one parameters or another depends on the mode and on the stiffnesses values of  $k_v^{b,2}$  and  $k_h^{b,2}$ . On the opposite, the

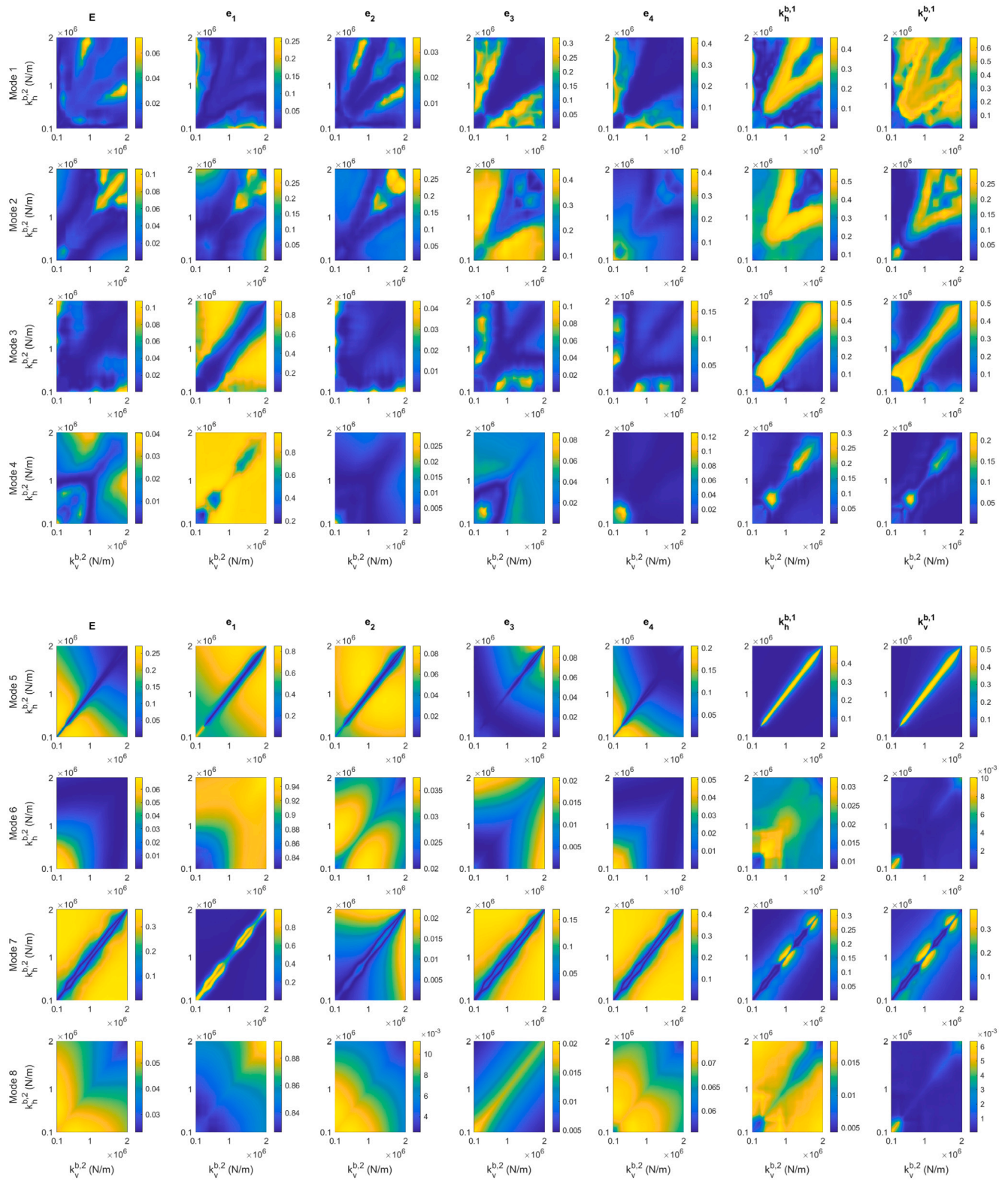


Fig. 12. First order Sobol indices of the modes 1 to 8 — Maximum amplitude.

total order Sobol indices are different from the first order ones, which demonstrates coupling effects between the different parameters. This is particularly observable on the Sobol indices of the stiffnesses  $k_v^{b,1}$  and  $k_h^{b,1}$  for the low backward modes. The following general observations can be made:

- mode 1: all parameters are influential in a part of the parametric space, but the two random stiffnesses prevail on the others. For the two stiffnesses, large coupling effects are present. These complex evolution and the presence of coupling effects illustrate the need for a high number of terms in the PCE.

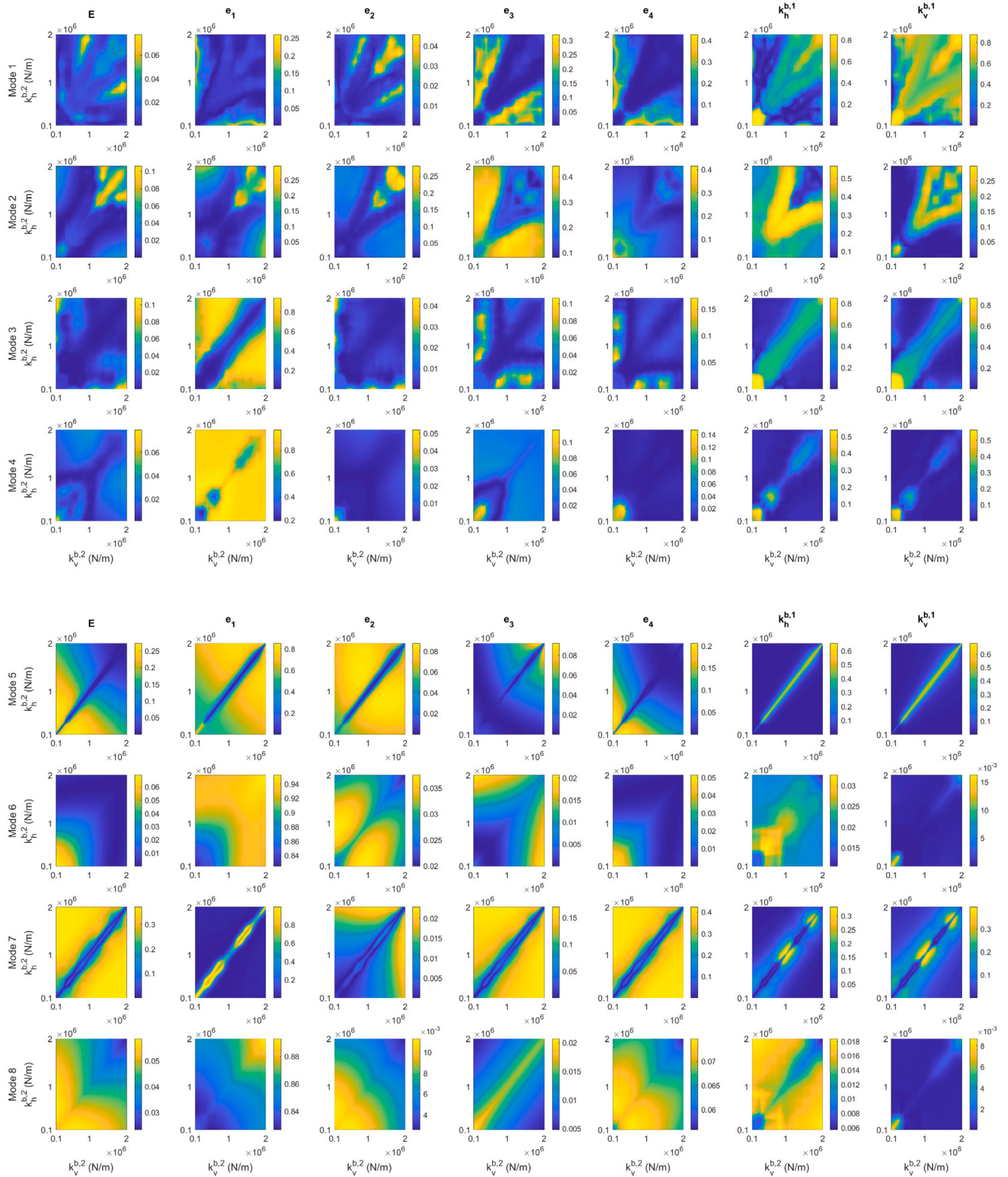


Fig. 13. Total order Sobol indices of the modes 1 to 8 — Maximum amplitude.

- mode 2: the two stiffnesses and the thickness of the third disc are the most influential parameters.
- mode 3: around the symmetry axis, the two stiffnesses are the most influential parameters, whereas otherwise the thickness of the first disc  $e_1$  has a major influence. If the major parameters are the same for the frequency and the amplitude, the area of influence of these parameters is different.
- mode 4: it is mostly driven by the thickness of the first disc over the whole parametric space.
- mode 5: on the symmetry axis, the two stiffnesses  $k_v^{b,1}$  and  $k_h^{b,1}$  are the dominating parameters. Otherwise, the thickness of the first disc  $e_1$  is the major parameter, followed by the Young modulus  $E$  and the thickness of the fourth disc  $e_4$  for low values of  $k_v^{b,2}$  and  $k_h^{b,2}$ . Similarly to mode 3, the main parameters are

same for the frequency and the amplitude, but not their area of influence.

- mode 6: the thickness of the first disc  $e_1$  is the parameter with the highest influence ( $S_{e_1}$  always superior to 0.8), and contributions from the other parameters are marginal. The difference between the role played by the different parameters compared to the frequency is clear here as only one parameter has a contribution for the amplitude and four of them where influential for the frequency.
- mode 7: on the symmetry axis, the thickness of the first disc is the most influential parameter, on the other parts of the parametric space, the  $E$ ,  $e_3$  and  $e_4$  are the main parameters.
- mode 8: the thickness of the first disc is the parameter that drives the amplitude for this mode.

As a more general comment, for higher modes, the stiffnesses  $k_v^{b,2}$  and  $k_h^{b,2}$  are the parameters that drive the symmetrical property of the rotor. Indeed, and even considering a loss of symmetry due to  $k_v^{b,1}$  and  $k_h^{b,1}$ , the average behaviour of the rotor does not change considerably. But for lower modes, even if  $k_v^{b,2}$  and  $k_h^{b,2}$  are equal then breaking the symmetry of the rotor with the stiffnesses of the first bearing support has a strong impact on the rotor dynamic and will increase drastically the vibration amplitudes. This is visible on Fig. 9 with the large variance, and in Fig. 12 with the large contribution of the two stiffness  $k_v^{b,1}$  and  $k_h^{b,1}$  around the diagonal. This effect is less visible for higher modes, and this is illustrated by the diminution of the influence area of  $k_v^{b,1}$  and  $k_h^{b,1}$ .

## 5. Conclusion

The present study proposes the application of a hybrid surrogate method for the prediction of the critical speeds and the associated amplitudes of the backward and forward modes of a complex rotor system. This study shows the potential of such approaches to effectively address the problem of rotor systems subject to a large number of uncertainties of different kinds such as random and parametric parameters.

The random parameters are modelled via a Polynomial Chaos Expansion whereas the two parametric parameters are modelled through a kriging strategy. The combination of Polynomial Chaos Expansions and kriging approach makes possible to process a considerable number of parameter sets and to perform calculations in a very reduced computational time compared to classical kriging approaches. Moreover, one of the interests of using kriging to predict PCE coefficients is to directly evaluate interesting characteristics such as the mean and variance of outputs of interests and to be able to perform a sensitivity analysis based on the calculation of Sobol indices.

Three different kriging strategies have been tested. Based on all the results for the estimation of both the frequencies of the critical speeds and the associated vibration amplitudes, it is observed that using known symmetric properties of the output results for the kriging construction allows a better prediction with less samples. This illustrates the need for a good understanding of the dynamic behaviour of the system of interest and a preliminary analysis of the desired output parameters for optimal construction of kriging meta-models. This also illustrates the advantage and the need to introduce in the meta-model the users knowledge of physics to achieve more efficient surrogate models.

The variance-based sensitivity analysis conducted illustrates the high variability of the vibration behaviours (i.e. the critical speeds and the associated amplitudes of the backward and forward modes) and the complex role played by the different random and parametric parameters.

Thus, this paper illustrates the current potential of the hybrid method based on the combination of the Polynomial Chaos Expansion and an “intelligent” kriging (in the sense of taking into account known symmetry properties of the initial physical problem and output results) as an efficient numerical tool for engineering design assistance and for a better understanding of the impact of different parameters on the dynamic behaviour of a rotating system.

## Declaration of competing interest

The authors declare that they have no known competing financial interests or personal relationships that could have appeared to influence the work reported in this paper.

## Acknowledgement

J.-J. Sinou acknowledges the support of the Institut Universitaire de France.

## References

- Barbosa, M.P.F., Alves, W.M., 2019. Kriging-based surrogate modeling for rotordynamics prediction in rotor-bearing system. In: Cavalca, K.L., Weber, H.I. (Eds.), Proceedings of the 10th International Conference on Rotor Dynamics – IFTOMM. Springer International Publishing, Cham, pp. 306–321.
- Barbosa, J.S., Sicchieri, L.C., Dourado, A., Jr., C., Jr., V.S., 2020. Kriging approach dedicated to represent hydrodynamic bearings. *J. Eng. Gas Turbines Power* 1197.
- Blatman, G., Sudret, B., 2011. Adaptive sparse polynomial chaos expansion based on least angle regression. *J. Comput. Phys.* 230 (6), 2345–2367.
- Denimal, E., Nechak, L., Sinou, J.-J., Nacivet, S., 2018. A novel hybrid surrogate model and its application on a mechanical system subjected to friction-induced vibration. *J. Sound Vib.* 434, 456–474.
- Denimal, E., Sinou, J.-J., Nacivet, S., 2019. Influence of structural modifications of automotive brake systems for squeal events with kriging meta-modelling method. *J. Sound Vib.* 463, 114938.
- Didier, J., Faverjon, B., Sinou, J.-J., 2012a. Analysing the dynamic response of a rotor system under uncertain parameters by polynomial chaos expansion. *J. Vib. Control* 18 (5), 712–732.
- Didier, J., Sinou, J.-J., Faverjon, B., 2012b. Study of the non-linear dynamic response of a rotor system with faults and uncertainties. *J. Sound Vib.* 331 (3), 671–703.
- Dupuy, D., Helbert, C., Franco, J., et al., 2015. DiceDesign and DiceEval: Two R packages for design and analysis of computer experiments. *J. Stat. Softw.* 65 (11), 1–38.
- Forrester, A., Sobester, A., Keane, A., 2008. Engineering Design Via Surrogate Modelling: A Practical Guide. John Wiley & Sons.
- Friswell, M.I., Penny, J.E., Garvey, S.D., Lees, A.W., 2010. Dynamics of Rotating Machines. Cambridge University Press, Cambridge, UK.
- Fu, C., Xu, Y., Yang, Y., Lu, K., Gu, F., Ball, A., 2020. Response analysis of an accelerating unbalanced rotating system with both random and interval variables. *J. Sound Vib.* 466, 115047.
- Garoli, G.Y., de Castro, H., 2020. Generalized polynomial chaos expansion applied to uncertainties quantification in rotating machinery fault analysis. *J. Braz. Soc. Mech. Sci. Eng.* 42 (5), 610.
- Han, F., Guo, X., Gao, H., 2013. Bearing parameter identification of rotor-bearing system based on Kriging surrogate model and evolutionary algorithm. *J. Sound Vib.* 332 (11), 2659–2671.
- Han, F., Guo, X., Mo, C., Gao, H., Hou, P., 2017. Parameter identification of nonlinear rotor-bearing system based on improved kriging surrogate model. *J. Vib. Control* 23 (5), 794–807.
- Huang, Z., Wang, C., Chen, J., Tian, H., 2011. Optimal design of aeroengine turbine disc based on kriging surrogate models. *Comput. Struct.* 89 (1), 27–37.
- Jacquelin, E., Friswell, M., Adhikari, S., Dessombz, O., Sinou, J.-J., 2016. Polynomial chaos expansion with random and fuzzy variables. *Mech. Syst. Signal Process.* 75, 41–56.
- Lophaven, S.N., Nielsen, H.B., Søndergaard, J., et al., 2002. DACE: A Matlab Kriging Toolbox, Vol. 2. Citeseer.
- Lu, Z., Lv, Y., Ouyang, H., 2019. A super-harmonic feature based updating method for crack identification in rotors using a kriging surrogate model. *Appl. Sci.* 9 (12), 2428.
- Lü, H., Yu, D., 2016. Optimization design of a disc brake system with hybrid uncertainties. *Adv. Eng. Softw.* 98, 112–122.
- Matheron, G., 1962. *Traité de Géostatistique Appliquée*. 1 (1962), Vol. 1. Editions Technip.
- Sarrouy, E., Dessombz, O., Sinou, J.-J., 2012. Stochastic analysis of the eigenvalue problem for mechanical systems using polynomial chaos expansion - Application to a finite element rotor. *J. Vib. Acoust.* 134 (5), 051009.
- Sinou, J.-J., Didier, J., Faverjon, B., 2015. Stochastic nonlinear response of a flexible rotor with local nonlinearities. *Int. J. Non-Linear Mech.* 74, 92–99.
- Sinou, J.-J., Jacquelin, E., 2015. Influence of polynomial chaos expansion order on an uncertain asymmetric rotor system response. *Mech. Syst. Signal Process.* 50, 718–731.
- Sinou, J.-J., Nechak, L., Besset, S., 2018. Kriging metamodeling in rotordynamics: Application for predicting critical speeds and vibrations of a flexible rotor. *Complexity* 1264619.
- Sobol, I.M., 1993. Sensitivity estimates for nonlinear mathematical models. *Math. Model. Comput. Exp.* 1 (4), 407–414.

- Sudret, B., 2008. Global sensitivity analysis using polynomial chaos expansions. *Reliab. Eng. Syst. Saf.* 93 (7), 964–979.
- Wang, D., Hua, C., Dong, D., He, B., Lu, Z., 2018a. Crack parameters identification based on a kriging surrogate model for operating rotors. *Shock Vib.* 9274526.
- Wang, L., Xiong, C., Yang, Y., 2018b. A novel methodology of reliability-based multidisciplinary design optimization under hybrid interval and fuzzy uncertainties. *Comput. Methods Appl. Mech. Engrg.* 337, 439–457.
- Wiener, N., 1938. The homogeneous chaos. *Amer. J. Math.* 60 (4), 897–936.
- Williams, C.K., Rasmussen, C.E., 2006. *Gaussian Processes for Machine Learning*, Vol. 2. MIT press, Cambridge, MA.
- Wu, J., Luo, Z., Li, H., Zhang, N., 2017. Level-set topology optimization for mechanical metamaterials under hybrid uncertainties. *Comput. Methods Appl. Mech. Engrg.* 319, 414–441.
- Xiu, D., Karniadakis, G.E., 2002. The Wiener–Askey polynomial chaos for stochastic differential equations. *SIAM J. Sci. Comput.* 24 (2), 619–644.
- Yongfeng, Y., Qinyu, W., Yanlin, W., Weiyang, Q., Kuan, L., 2019. Dynamic characteristics of cracked uncertain hollow-shaft. *Mech. Syst. Signal Process.* 124, 36–48.
- Zhang, Z., Ma, X., Hua, H., Liang, X., 2020. Nonlinear stochastic dynamics of a rub-impact rotor system with probabilistic uncertainties. *Nonlinear Dynam.* 102, 2229–2246.
- Zheng, J., Luo, Z., Jiang, C., Gao, J., 2019. Robust topology optimization for concurrent design of dynamic structures under hybrid uncertainties. *Mech. Syst. Signal Process.* 120, 540–559.